MICROSTRUCTURAL AND MECHANICAL PROPERTIES OF HUMAN RIBS

JOSEPH MICHAEL CORMIER

Thesis submitted to the Faculty of the
Virginia Polytechnic Institute and State University
in partial fulfillment of the requirements for the degree of

Master of Science
in
Mechanical Engineering

Stefan M. Duma, Ph.D., Chair
Michael L Madigan, Ph.D.
Ian P. Herring, D.V.M.

April 22, 2003

Blacksburg, Virginia

Keywords: Bone, Impact, Osteon, Rib, Thorax,

MICROSTRUCTURAL AND MECHANICAL PROPERTIES OF HUMAN RIBS

Joseph Michael Cormier

(ABSTRACT)

Determining the risk of injury from an automobile collision to the thorax requires knowledge of the properties of the skeletal components that comprise the thorax. The direction of osteons in cortical bone has been shown to be well correlated with the strongest loading direction of the bone as a whole. Therefore, determining the orientation of osteons in the rib cage is an important step in understanding the behavior of the rib cage under mechanical load. Histological slides were created in series from various regions of the each rib in the thorax. Image analysis of the digitized histology sections included the use of a computer algorithm created in Matlab to track the center of each osteon throughout the rib section. Analysis of the results showed variations in the osteon direction between samples taken from the anterior, lateral and posterior surfaces of the rib cage. The results indicate a trend in osteon offset angle between the three locations studied. The second purpose of this study was to investigate the strength of human ribs subjected to dynamic three-point bending. For all subjects, the anterior specimens failed at a significantly lower peak stress than the lateral ($p=0.01$) and posterior ($p=0.01$) specimens. The average elastic modulus from all tests was 22 GPa. The results of this study suggests that there are variations in the mechanical properties of the rib cage. These variations need to be considered when developing an accurate method of thoracic injury prediction.

Acknowledgements

The research described here was made possible through contributions from lab mates, family members and friends. The Impact Biomechanics Lab presented a great learning environment thanks to Carla Wilhoit, Dave Moorcroft, Dave Tordonato, Eric Kennedy, Gail Hansen, Ginny Jernigan, Joel Stitzel, Katherine Voorhies and Will Hurst. Special thanks goes to Dave M., Joel and Will for the morning coffee conversations.

Stefan Duma provided excellent academic support and guidance as my advisor, and above all made me a better person and a more capable engineer.

I would also like to thank Ian Herring and Michael Madigan for their excellent help and support on my research as well as serving on my graduate committee.

Thanks to my friends for the worthwhile distractions and for buying my beer because I was a poor student. In particular, I would like to thank Dr. Grey Heyt for his outstanding support and guidance.

To my sister Jessica for reminding me to take a break and have fun, and my parents for reminding me not to have too much fun – words can't express what you mean to me.

TABLE OF CONTENTS

LIST OF FIGURES

LIST OF TABLES

Chapter 2

Chapter 3

CHAPTER 1

Introduction

The human thorax serves an essential purpose by protecting vital organs responsible for the circulation and respiration of the individual. Any injury to its components can have a direct effect on the performance of these organs that are essential to life. It is for these reasons that the human thorax is the focus of the current research.

The purpose of this study was to determine the correlation between microstructural characteristics of the human rib and their response during dynamic three-point bending. Dynamic bending was chosen to gain a better understanding of the viscoelastic properties of human ribs. Strength characteristics under dynamic loading are important for the development of injury criteria that are used in a wide range of applications, one of which being automotive safety restraints.

Previous research performing impact sled tests on cadaver subjects have frequently found rib fracture to be the most common skeletal injury (Alem 1978, Crandall 1997, Kallieris 1998, Cromack 1975, Patrick 1967, 1974, Ramet 1979). This is concurrent with a survey of the National Automotive Sampling System (NASS) performed by Crandall *et al.* (1994). Projected national trends for occupants incurring an Abbreviated Injury Score or AIS $\geq$ 3 in the years 1984 thru 1992 indicated that thoracic injuries were the second most common injury among 2 and 3 point belt wearers. A thoracic injury of an AIS $\geq$ 3 would indicate an occupant incurring at least 3 to 4 rib fractures. A survey of 314 occupants in automotive accidents showed that rib fracture was the most common skeletal injury (Dalmotas 1980). The high occurrence rate of rib fracture suggests that there is room for improvement in the current state of automotive restraint technology.

The results of whole cadaver studies can be used to develop predictive functions for the number of rib fractures an occupant may incur during an automotive collision (Cesari 1990, Eppinger 1978, 1984, Kallieris 1974, 1998, Kuppa 1998, Nahum 1975, Viano 1978, Walfisch 1985). These predictive functions are based on parameters such as: viscous criterion, chest acceleration, age and chest deflection. However, they give little insight into the strength of the skeletal components that make up the thorax. This type of information is essential for the development of finite element models used to predict skeletal injury for evaluating restraint systems.

The information gained during this study is essential for the improvement of predictive models used for the analysis of safety restraints and various applications in which injury tolerance of the thorax is needed. The microstructural analysis of rib sections from two human cadavers will be discussed as well as the results of 59 dynamic three-point bending tests performed on rib sections from 4 cadaver subjects. Various components of bone microstructure have been shown to correlate with the stronger loading directions of bone. Therefore, by determining the preferred orientation of microstructure in the human rib, any anisotropic behavior or lack thereof may be explained. The sections to follow in this chapter are brief descriptions of the relevant thoracic anatomy and bone microstructure.

The algorithms created in Matlab to perform the histological analysis are included in Appendix (A).

Background

Thorax

The thorax is comprised of ribs, thoracic vertebrae, costal cartilage and the sternum. The 12 thoracic vertebrae (T1-T12) and the corresponding ribs form the posterior side of the thorax. Each rib articulates with respect to the vertebrae to facilitate respiration. The anterior surface is formed by the sternum and costal cartilage. The costal cartilage forms a bridge between the central sternum and the first ten ribs. The first seven pairs of ribs connect directly to the sternum through costal cartilage, creating true ribs. The following three pairs join together by costal cartilage then attach to the sternum. The two remaining pairs are not attached to the sternum and are termed floating ribs. The curvature of the ribs themselves is greatest for the first rib, then decreases for the lower ribs (Figure 1).

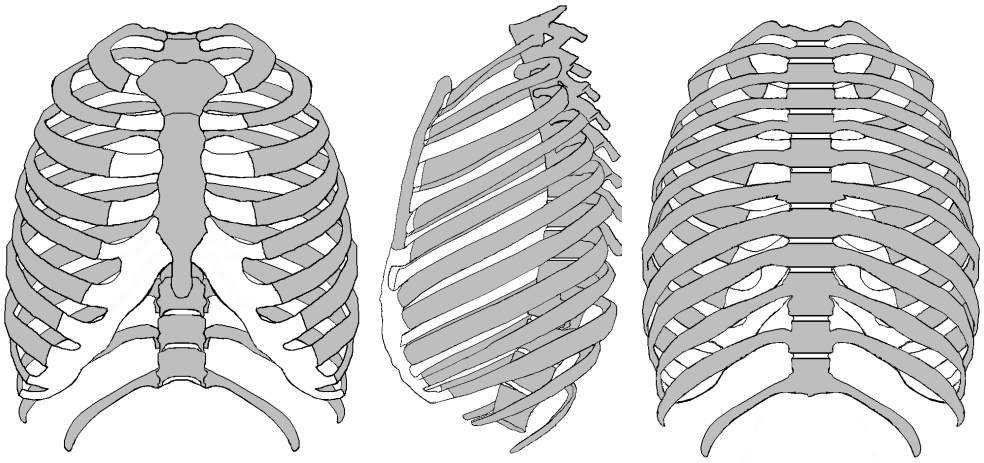

Figure 1: Anterior (left), lateral and posterior (right) view of the thorax (Costal cartilage is shown in white).

The sternum is comprised of three parts. The manubrium, gladiolus and xiphoid appendix form the upper, middle and lower portions of the sternum, respectively. The manubrium forms the articulating surface with the costal cartilage of the first rib and

creates half of the articulating surface for the second rib. The remaining half of the articulating surface is created by the middle portion of the sternum, the gladiolus. The gladiolus is the largest of the three portions and contains the articulating surface for the second through the seventh ribs. The xiphoid appendix forms the lower portion of the articulating surface of the seventh rib.

The articulations between the true ribs and the sternum are created by arthrodial joints. The first rib is the exception, in which case the rib and sternum are directly united by cartilage creating a synarthrodial articulation. The remaining second through seventh ribs are attached to the sternum via six ligaments. The resulting arthrodial joints permit little if any motion of the sternum end of the rib with respect to the sternum body. The costal cartilages of the sixth through tenth rib are connected to each other via intra-chondral ligaments. The sixth through ninth ribs have an additional attachment through intercostals synovial membranes, creating a more rigid bond between these ribs.

From the sternum, the ribs form the lateral and posterior portion of the thorax and then attach to the spine in one of two different variations of attachment sites. In the case of the second through ninth ribs, the attachments are made at the junction between two vertebral bodies. In the remaining ribs (1^{st},10^{th}, 11^{th}, 12^{th}) the cavity in which the rib attaches is formed by a single vertebrae. The eleventh and twelfth ribs articulate only between the head and the vertebral body. All other ribs articulate in this manner as well as between the tubercles and neck of the rib with the transverse process of the vertebral body. There are three ligaments creating the first type of joint and four creating the second. This makes a total of seven ligaments involved in the connection between the second through tenth ribs with the vertebra (Gray 1995).

The joints between the vertebra and ribs allow more motion than those at the sternum. This is necessary to facilitate respiration by allowing the ribs to move and altering the total volume of the thorax. The allowable motion of the ribs with respect to the vertebrae increases downward along the spine, with the eleventh and twelfth ribs being the most mobile in terms of the joint itself.

The mechanical aspects of the ribs and their articulations between the sternum and vertebrae are an important part of this study. The articulations between each rib and the sternum create a fixed type of end condition. This fixed end condition allows the production of a bending or torsional moment at the attachment site. This may prove to be an important factor when considering the effects this may have in the way the microstructure of the rib adapts during the life of an individual. The articulations of the ribs with the vertebral column may be classified as more of a pinned condition. This condition allows the rib to rotate slightly, but translation is limited, therefore, the production of torsional forces in the posterior portion of the rib is limited. The differences between the articulations of the rib at each end may effect the microstructural adaptation that occurs during life.

Bone Microstructure

The human rib is composed of cancellous bone surrounded by a thin cortical shell. The cancellous core is created by an array of plates and columns of trabeculae. This produces a structure with variable porosity and intercommunicating pores filled with bone marrow. The classification of bone from compact to cancellous is dependent on its porosity. The range of porosity for compact bone is 5% to 30% and 30% to over 90% for cancellous bone (Carter and Hayes 1977). Cortical bone is responsible for providing the

majority of the strength for the rib, particularly in tension and therefore is the focus of this study.

Cortical bone is made of an array of Haversian systems or osteons, that are connected together by lamellar bone. A single osteon is comprised of a central canal, or Haversian canal, that contains circulatory structures though the cortical bone. The Haversian canal is then surrounded by concentric lamellae, or Haversian lamellae. Osteocytes are contained within lacuna that exist among the layers of concentric lamellae. The outer ring of the osteon is connected to surrounding osteons and lamellar bone through cement lines (Figure 2).

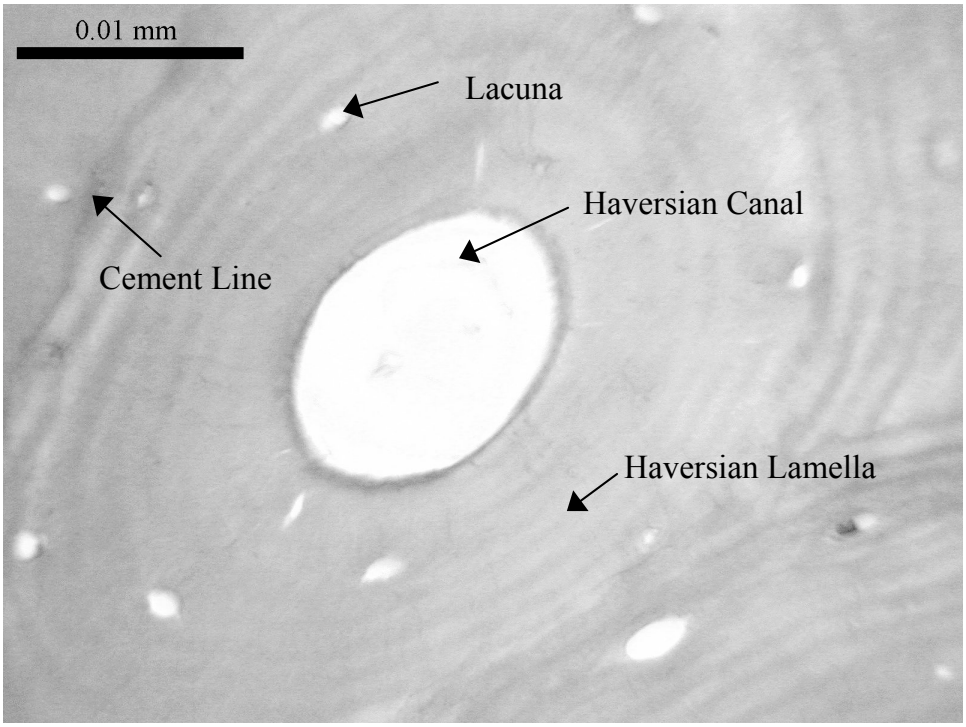

Figure 2: Single Haversian system of rib specimen used in current study.

The response of bone to externally applied forces is a function of its composition on a microscopic level. The strength of an entire rib, for example, is dependent on the arrangement of osteons in the cortical shell and trabeculae in the cancellous core. Small

scale testing, whether it is performed on isolated osteons, or specimens of cortical or cancellous bone can provide essential information on the strength of any bone as a whole. The orientation of the osteons in the cortical shell has been of significant importance to previous investigators, as its been shown that the orientation of osteons corresponds to the stronger direction of cortical bone (Hert 1998, 1994, Black 1980, Pfeiffer 1998, Pidaparti 1992). To the best of the authors' knowledge, no previous work has been performed to determine the orientation of osteons in the human rib.

Knowing the orientation of osteons in human ribs may also give insight into the intrinsic adaptation processes that occur *in vivo*. Previous research has provided insight into the adaptation of bone through changes in the orientation of trabeculae, (Cowin 1986, Hayes 1978, Wolff 1892) bone density (Bobyn 1992, Fyhrie 1990, Krall 1994) and bone geometry (Forwood 1993, Kannus 1996, Martin 1977, Ruff 1988). Previous research on human femoral bone has shown that trabecular eccentricity exists at the femoral neck (Bell 1996, 1999, Boyce 1993, Demes 2000, Komatsu 1998, Ohman 1997, Rafferty 1998, Yoshikawa 1994). Trabecular eccentricity is the non-uniform distribution of cortical bone thickness about the circumference of the bone. The effects of this asymmetrical distribution of cortical bone in the femoral neck was investigated by Fox *et al.* (2001). Their results indicated that an increase in trabecular eccentricity lowered the risk of fracture at the femoral neck. In part, this was due to a thickening of the cortical bone at regions of the femoral neck subjected to compression. Turner *et al.* (1998) proposed three rules for the causes of bone adaptation. First, it is driven by dynamic mechanical stimulus rather than static. Second, only short durations of mechanical loading is necessary to initiate remodeling. Finally, bone cells will respond less to more routine loading. It is important to

consider the remodeling aspect of bone for this study because otherwise, the orientation of osteons in the cortical bone of the ribs would seem to be of little importance.

Cortical bone is formed through the combination of osteons and lamellar bone as previously described. The adaptation of cortical bone has been shown to be a result of the growth of secondary osteons through primary bone (Bain 1990, Bouvier 1981,1996, Burr 1985, 1989, 1993, Carter 1984, 1987, Hert 1972, Hylander 1979,1991, Lanyon 1976,1984,1993, Martin 1992, Rubin 1988). It is the orientation of these osteons that are responsible for the mechanical characteristics of cortical bone. Therefore, an improved understanding of how cortical bone adapts may be determined by knowing the orientation of osteons in cortical bone.

The orientation of osteons dictates the preferred loading direction of the bone and therefore provides insight into the mechanical loading of the bone *in vivo*. Previous research on bone adaptation provides proof of its existence and, therefore, knowledge of the orientation of new bone formed by secondary osteons can be used to reinforce isotropic properties determined through mechanical testing. However, the actual strength of the bone can only be determined through mechanical testing methods. Knowledge of the microstructural and mechanical properties of the human rib may be used together to account for strength variations that occur between ribs at each level as well as sections of a single rib.

The objectives of this study are as follows:

1. To investigate the variation in osteon orientation between ribs at different levels of the thorax as well as variations within the length of the rib themselves.
2. To investigate the dynamic bending properties of human ribs at each level of the thorax as well as at different locations of a single rib.

References

Alem NM, Bowman BM, Melvin JW, Benson JB: Whole-Body Human Surrogate Response to Three-Point Harness Restraint, Proceedings of the 22nd Stapp Car Crash Conference, Society of Automotive Engineers, 780895; 1978.

Bain S.D. Rubin C.T.: Metabolic Modulation of Disuse Osteopenia: Endocrine-Dependent Site Specificity of Bone Remodeling. *J. Bone Min. Res.,* 5: 1069-1075; 1990.

Bell K.L., Garrahan N., Kniessel M., Loveridge N., Grau E., Stanton M., Reeve J.: Cortical and Cancellous Bone in the Human Femoral Neck: Evaluation of an Interactive Image Analysis System. *Bone,* 19: 541-548; 1996.

Bell K.L., Loveridge N., Power J., Garrahan N., Stanton M., Lunt M., Meggitt B.F., Reeve J.: Structure of the Femoral Neck in Hip Fracture: Cortical Bone Loss in the Inferoanterior to Superoposterior Axis. *J. Bone Miner. Res.,* 14: 111-119; 1999.

Black J, Richardson SP, Mattson RU, Pollack SR: Haversian Osteons: Longitudinal Variation of Internal Structure. J Biomed. Mat. Res., 14: 41-53; 1980.

Bobyn J.D., Mortimer E.S., Glassman A.H., Engh C.A., Miller J.E., Brooks C.E.: Producing and avoiding stress shielding. Laboratory and Clinical Observations of Noncemented Total Hip Arthroplasty, *Clin. Orthop.,* 274: 79-96; 1992.

Bouvier M., Hylander W.L.: Effect of Bone Strain on Cortical Bone Structure in Macaques. *J. Morphol.,* 167: 1-12; 1981.

Boyce T., Bloebaum R.: Cortical Aging Differences and Fracture Implications for the Human Femoral Neck. *Bone* 14: 769-778; 1993.

Burr D.B., Martin R.B., Schaffler M.B., Radin E.L.: Bone Remodeling in Response to *In Vivo* Fatigue Microdamage. *J. Biomech.,* 18: 189-200; 1985.

Burr D.B., Schaffler M.B., Yang K.H., Wu D.D., Lukoschek M., Kandzari D., Sivaneri N., Blaha J.D., Radin E.L.: The Effects of Altered Strain Environments on Bone Tissue Kinetics. *Bone,* 10: 215-221; 1989.

Burr D.B.: Remodeling and the Repair of Fatigue Damage. *Calcif. Tissue Int.,* 53: S75-S81; 1993.

Carter D.R.: Mechanical Loading Histories and Cortical Bone Remodeling. *Calcif. Tissue Int.,* 36: S19-S24; 1984.

Carter D.R.: Mechanical Loading History and Skeletal Biology. *J. Biomech.,* 20: 1095-1109; 1987.

Carter DR, Hayes WC: The Compressive Behavior of Bone as a Two-Phase Porous Structure. J. Bone J. Surg.,59: 954-62; 1977.

Cesari D, Bouquet R: Behavior of Human Surrogates Thorax under Belt Loading. Proceedings of the 34th Stapp Car Crash Conference, Society of Automotive Engineers. 73-81, 902310; 1990.

Cowin S.C.: Wolff's Law of Trabecular Architecture at Remodeling Equilibrium. *J. Biomech. Eng.,* 108: 83-88; 1986.

Crandall JR, Bass CR, Pilkey WD, Miller HJ, Sikorski J, Wilkins M: Thoracic Response and Injury with Belt, Driver Side Airbag and Force Limited Belt Restraint Systems. International Journal of Crashworthiness, 2(1): 119-132; 1997.

Crandall JR, Pilkey WD, Klopp GS, Sieveka E, Morgan R, Eppinger R, Kuppa S, Grove C: A Comparison of Two and Three Point Restraint Systems. Joint AAAM-IRCOBI Session, Sept. 22; 1994.

Cromack JR, Ziper HH: Three-Point Belt Induced Injuries: A Comparison Between Laboratory Surrogates and Real World Accident Victoms. Proceedings of the 19th Stapp Car Crash Conference, Society of Automotive Engineers., 751141: 1-22; 1975.

Dalmotas DJ: Mechanisms of Injury to Vehicle Occupants Restrained by Three-Point Seat Belts, Proceedings of the 24th Stapp Car Crash Conference, Society of Automotive Engineers, 801311; 1980.

Demes B., Jungers W.L., Walker C.: Cortical Bone Distribution in the Femoral Neck of Strepsirhine Primates. *J. Hum. Evol.,* 39: 367-379; 2000.

Eppinger RH, Augustyn K, Robbins DH: Development of a Promising Universal Thoracic Trauma Prediction Methodology. Proceedings of the 22nd Stapp Car Crash Conference, Society of Automotive Engineers, 780891; 1978.

Eppinger RH, Marcus JH, Morgan RM: Development of Dummy and Injury Index for NHTSA's Thoracic Side Impact Protection Research Program. Proceedings of the Gover./Industry, Expo, Society of Automotive Engineers, 840885; 1984.

Forwood M.R., Burr D.B.: Physical Activity and Bone Mass: Exercises in Futility? *Bone Miner.,* 21: 89-112; 1993.

Fox J.C., Keaveny T.M.: Trabecular Eccentricity and Bone Adaptation. *J. Theor. Biol.,* 212: 211-221; 2001.

Fyhrie D.P., Carter D.R.: Femoral Head Apparent Density Distribution Predicted from Bone Stresses. *J. Biomech.,* 23: 1-10; 1990.

Gray H. Gray's Anatomy. 15th Ed. Barnes & Noble Books, New York, NY; 1995.

Hayes W.C., Swenson L.W., Schurman D.J.: Axisymmetric Finite Element Analysis of the Lateral Tibial Plateau. *J. Biomech.,* 11: 21-22; 1978.

Hert J, Fiala P, Petrtyl M: Osteon Orientation of the Diaphysis of the Long Bones in Man. Bone, 15(3): 269-277; 1994.

Hylander W.L., Rubin C.T., Bain S.D., Johnson K.R.: Correlation Between Haversian Remodeling and Strain Magnitude in the Baboon Face. *J. Dent. Res.,* 70: 360; 1991.

Hylander W.L.: The Functional Significance of Primate Mandibular Form. *J. Morphol.,* 160: 223-340; 1979.

Kallieris D, Schmidt G, Barz J, Mattern R, Schulz F: Response and Vulnerability of the Human Body at Different Impact Velocities in Simulated Three-Point Belted Cadaver Tests. IRCOBI, 196-209; 1974.

Kallieris D, Zerial PD, Rizzetti A, Mattern R: Prediction of Thoracic Injuries in Frontal Collisions. Enhanced Safety of Vehicles, 98-S7-O-04: 1550-63; 1998.

Kannus P., Sievanen H., Vuori I.: Physical Loading, Exercise, and Bone. *Bone* 18: S1-S3; 1996.

Komatsu T.: Morphological Studies of the Upper End of the Femur II. Macroscopic, Radiological, Histological and Hostomorphometrical Studies. *J. Jpn. Orthop. Assoc.,* 62: 1029-1041; 1998.

Krall E.A., Dawson B.: Walking is Related to Bone Density and Rates of Bone Loss. *Am. J. Med.,* 96: 20-26; 1994.

Kuppa S, Eppinger R: Development of an Improved Thoracic Injury Criterion. Proceedings of the 42nd Stapp Car Crash Conference, Society of Automotive Engineers, 983153; 1998.

Lanyon L.E., Baggott D.G.: Mechanical Function as an Influence on the Structure and Form of Bone. *J. Bone Joint Surg.,* 58B: 436-443; 1976.

Lanyon L.E., Rubin C.T.: Static vs Dynamic Loads as an Influence on Bone Remodeling. *J. Biomech.,* 17: 897-905; 1984.

Lanyon L.E.: Osteocytes, Strain Detection, Bone Modeling and Remodeling. *Calcif. Tisssue Int.,* 53: S102-S106; 1993.

Martin R.B., Atkinson P.J.: Age and Sex-Related Changes in the Structure and Strength of the Human Femoral Shaft. *J. Biomech.,* 10: 223-231; 1977.

Martin R.B.: A Theory of Fatigue Damage Accumulation and Repair in Cortical Bone. *J. Orthopaed. Res.,* 10: 818-825; 1992.

Nahum AM, Schneider DC, Kroell CK: Cadaver Skeletal Response to Blunt Thoracic Impact. Proceedings of the 19th Stapp Car Crash Conference, Society of Automotive Engineers 259-277, 751150; 1975.

Ohman J.C. Krochta T.J., Lovejoy C.O., Mensforth R.P., Latimer B.: Cortical Bone Distribution in the Femoral Neck of Hominoids: Implications for the Locomotion of Australopithecus Afarensis. *Am. J. Phys. Anthrop.,* 104: 117-131; 1997.

Patrick LM, Anderson A, Bohlin N: Three-Point Harness Accident and Laboratory Data Comparison. Proceedings of the 18th Stapp Car Crash Conference, Society of Automotive Engineers, 741181; 1974.

Patrick LM, Kroell CK, Mertz HJ: Cadaver Knee, Chest and Head Impact Loads. Proceedings of the 11th Stapp Car Crash Conference, Society of Automotive Engineers, 670913: 168-82; 1967.

Pfeiffer S: Variability in Osteon Size in Recent Human Populations. Amer. J. Phys. Anthropol., 106: 219-27; 1998.

Pidaparti RMV, Burr DB: Collagen Figer Orientation and Geometry Effects on the Mechanical Properties of Secondary Osteons. J Biomech, 25(8): 869-80; 1992.

Rafferty K.: Structural Design of the Femoral Neck in Primates. *J. Hum. Eval.* 34: 361-383; 1998.

Ramet M Cesari: Behaviour of Restrained Dummies and Cadavers in Frontal Impacts. IRCOBI: 210-19; 1979.

Rubin C.T. Housman M.R.: The Cellular Basis of Wolff's Law. Transduction of Physical Stimuli to Skeletal Adaptation. *Rheum. Dis. Clin. North. Am.,* 14: 502-517; 1988.

Ruff C.B., Hayes W.C.: Sex Differences in Age-Related Remodeling of the Femur and Tibia. *J. Orthop. Res.,* 6: 886-896; 1988.

Turner C.H. Three Rules for Bone Adaptation to Mechanical Stimuli. *Bone,* 23(5): 399-407; 1998.

Viano DC, Warner CY, Hoopes K, Morenson C, White R, Artinian CG: Sensitivity of Porcine Thoracic Responses and Injuries to Various Frontal and A Lateral Impact Site. Proceedings of the 22th Stapp Car Crash Conference, Society of Automotive Engineers. 169-207, 780890; 1978.

Walfisch G, Chamouard F, Lestrelin D, Tarriere C, Cassan F, Mack P, Got C, Guillon F, Patel A, Hureau J: Predictive Functions for Thoracic Injuries to Belt Wearers in Frontal Collisions and Their Conversion into Protective Criteria. Proceedings of the 29th Stapp Car Crash Conference, Society of Automotive Engineers, 851722; 1985.

Wolff J.: *Das Gesetz der Transformation der Knochen.* Berlin: Hirschwald; 1892.

Yoshikawa T., Turner C.H., Peacock M., Slemenda C.W., Weaver C.M., Teegarden D., Markwardt P., Burr D.B.: Geometric Structure of the Femoral Neck Measured Using Dual-Energy X-ray Absoptiometry. *J. Bone Miner. Res.,* 9: 1053-1064; 1994.

CHAPTER 2

Orientation of Osteons in the Human Rib Cage

Abstract

The direction of osteons in cortical bone has been shown to be well correlated with the strongest loading direction of the bone as a whole. Therefore, determining the orientation of osteons in the rib cage is an important step in understanding the behavior of the rib cage under mechanical load. A total of 37 specimens were removed from several rib locations from a male and female cadaver. Eight histological slides were created from each 5 mm long section. Image analysis included the use of a computer algorithm created in Matlab to track the center of each osteon throughout the rib section. Analysis of the results showed variations in the osteon direction between samples taken from the anterior, lateral and posterior surfaces of the rib cage. The average offset angle between the osteon direction and the rib axis was determined to be 4.1, 3.2 and 1.9 degrees for the anterior, lateral and posterior surfaces respectively. The average offset angle for the anterior specimens was significantly higher than that of the posterior rib specimens (P=0.01) The lateral specimens also showed a significantly higher average offset angle than the posterior rib specimens (P=0.01). The results indicate a trend in osteon offset angle between the three locations studied. The offset angle is highest in the anterior region, then decreases in the lateral and is lowest in the posterior regions of the rib cage.

Introduction

Bone microstructure and its orientation play an important role in determining the response of the bone as a whole. Specifically, knowing the orientation of osteons in cortical bone is an important part in understanding the adaptation of bone to mechanical

forces. The orientation of osteons may also give insight into the anisotropic behavior of bone.

The majority of previous work has focused on the microstructure of the long bones in human and animal models. Much of the early work on the orientation of osteons have found conflicting results as to whether or not osteons show a preferred direction other than the long axis of the bone (Hert 1994). Work showing an oblique osteon orientation began with Cohen and Harris in 1958. Their analysis of the canine femur showed a helical direction of the osteons about the bone circumference. This finding was reinforced later by Martin and Burr (1989). The oblique orientation of the osteons with respect to the long axis was also supported by Black *et al.* in 1980 using human tibial specimens. The average angle of inclination with respect to the long axis of the bone was found to be 5.45 degrees. Work by Tappen (1977) did not show that osteons assumed an oblique pattern with respect to the bone axis. This is difficult to accept due to previous work described here that did find an oblique orientation of osteons in cortical bone. The results of Tappen (1977) also deviate from the accepted belief that bone adapts to forces it is exposed to *in vivo* (Cowin 1986, Hayes 1978, Wolff 1892). The adaptation of cortical bone has been shown to take place through the growth of secondary osteons in cortical bone (Burr 1993, Carter 1984, Martin 1992, Rubin 1988). Therefore, these osteons should deviate from the long axis of the bone in the human skeleton, due to the complex loading conditions placed on bone during motion.

The influence of osteon direction on the mechanical properties of bone was shown by Petrtỳl (1988), Lanyon and Bourn (1979) as well as Hert *et al.* (1994). Petrtỳl found the elastic modulus of the human femur to be highest in the helical directions described by

previous researchers as the direction of osteons in the femur. More recently, the orientation of osteons in the humerus, radius, ulna, tibia, and femur were examined by Hert *et al.* (1994). The authors observed a 5 to 15 degree offset of the osteons from the long axis of the bone. The cortical bone exhibited sharp boundaries between osteons of different orientation. Hert also showed that the offset angle of the osteons matched the direction of the principal strains in the bone under a combination of bending and torsional loading. Lanyon and Bourn (1979), as a result of their study of sheep tibia found an oblique orientation of osteons that resemble those found later by Hert *et al* (1994). This orientation coincided with the direction of principal strains under the bending and torsional loading condition as well. The adaptation of cortical bone itself by the growth of secondary osteons supports the importance of knowing the orientation of osteons in the human rib cage.

The purpose of this study was to investigate the orientation of osteons in the human rib cage. This was performed in hopes of expanding the current understanding of the behavior of the rib cage under mechanical load, and the adaptation provided by the osteons. The ribs represent a unique piece of the human skeleton, in that they are continuously loaded by the forces necessary for respiration. Therefore, the articulations of the ribs with the sternum and vertebral bodies play an influential role in the microstructural adaptation of the ribs.

Methodology

Two cadavers were used for this study, a 71 year old male and a 61 year old female. Rib sections were removed from each of the two cadavers using an autopsy saw. A total of 19 and 18 sections were removed from ribs on the left side of the thorax for a female and male

subject respectively (Figure1). For the female, subject eight histological slides were created from each rib section removed from the thorax at various locations. For the male subject, nine histological slides were created from each of the 18 rib specimens. The combination of these resulted in a total of 152 histological slides for the female and 162 slides for the male subjects.

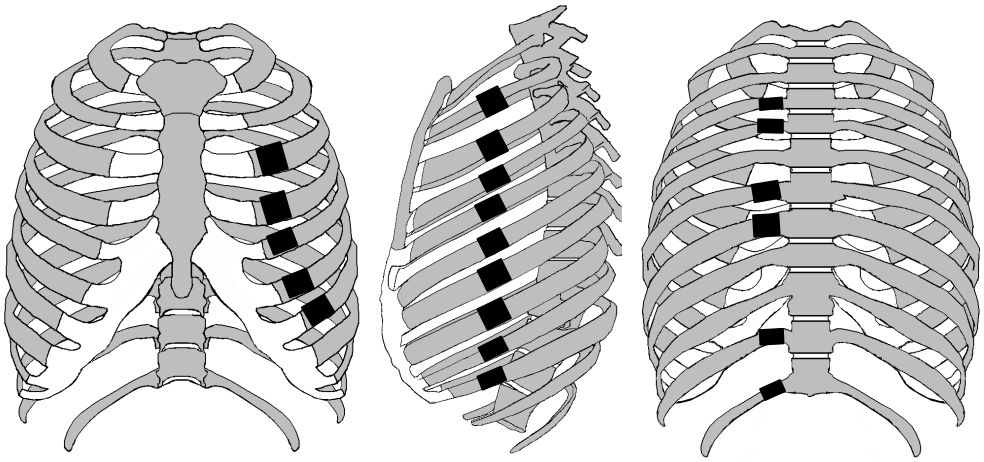

Figure 1: Locations from which sections were removed for histological analysis.

These sections were then cut again to reduce the specimens to a length of 3 mm. These secondary cuts were performed using a low speed diamond saw (Model 650 South Bay Tech. California, USA) equipped with a specially designed bone chuck and saline bath, thereby, producing a specimen with parallel edges while minimizing any mechanical damage induced during the cutting process. Once the specimen was reduced to its final length, two cuts were made in the cortical bone of the specimen that served as reference markers for histological analysis. These cuts were made in the interior and superior surface of the bone, using the low speed saw (Figure 2). The rib sections were then submerged in a 10% buffered Formalin solution to prevent decomposition of the bone until histological sectioning was performed.

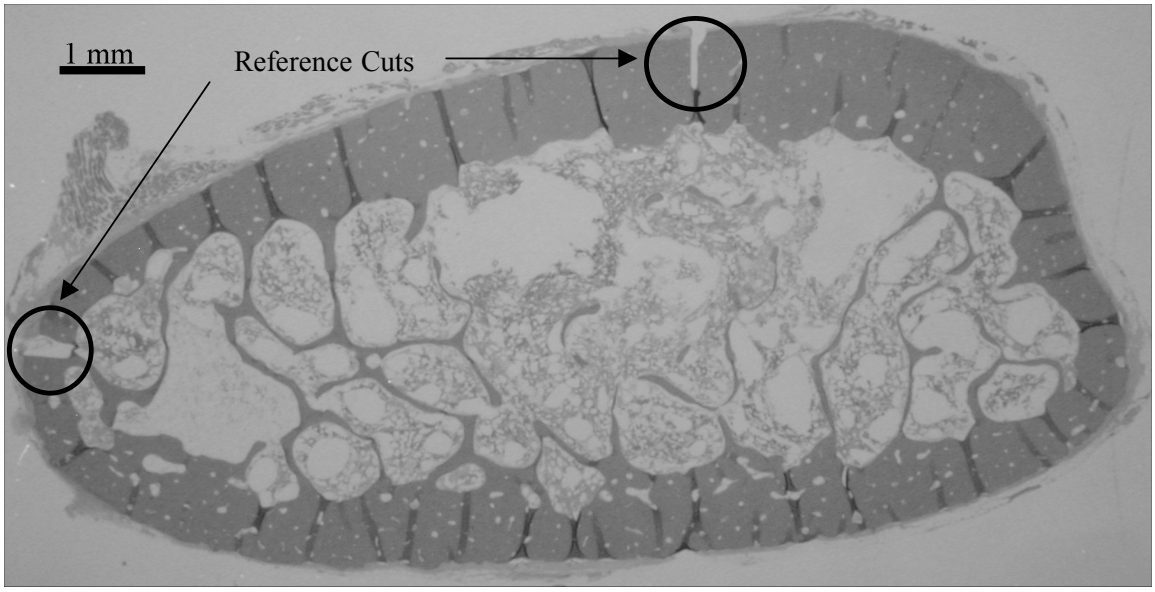

Figure 2: Histological slide of rib section with interior surface at the top and superior surface at the left side of the image.

Histological sectioning began by dividing the 3 mm rib specimens into 8 levels with a distance of 300 microns between each level for the female subject. The 3 mm specimens from the male subject were divided into 9 levels with the same 300 micron distance between each level. Two slices were taken at each of these levels at a slice thickness of 4 microns. Creating two slices at each level is not necessary, however, this increases the probability of having a useable histology slice at each level.

Once the histology slides were received, one image at each level was created for processing. This was done using a bifocal microscope (Model LEG 05 ,Wild Heerbrugg, Switzerland) equipped with a digital camera (Model 3500, Nikon, Melville, NY). A magnification of 8-10 times was used to ensure that the Haversian canals in the cortical bone were visible. The camera was set to a resolution of 2048 by 1536 and the images were saved in Tagged Image File (tif) format. Digitized images of an objective micrometer were also taken in order to convert lengths measured in pixels to millimeters.

Processing the images began by converting them to black and white images. This reduced the color depth of the images to 1 bit meaning that the images were basically an array of ones and zeros, one indicating white and zero indicating black. The center of each osteon in the cortical bone is marked by the Haversian canal (Hert 1994). After creating histological slides of the rib cross section, these canals are visible as holes, or white areas in a black and white image. The trabeculae of the cancellous bone created a similar appearance, so to avoid erroneous results, the cancellous portion of each image was digitally removed. This created an image of a large white void in the center of the cortical shell that was then analyzed using computer algorithms.

Multiple algorithms were created in Matlab (Release 12, The Mathworks, Natick, MA) to load and process the black and white image of the histological sections. The first algorithm identified each Haversian canal and then determined its geometric center. This produced an array of x,y coordinates of the center position of the Haversian canals in the image. Due to slight differences in the position of the rib section when the image was created, the x,y coordinates from each image can only be applied to their respective image. To correct this, the location of the reference cuts on the rib surface are used as datum markers for each section. The location of these cuts were consistent throughout the section. By digitally re-aligning these reference cuts, each histological image could be viewed with respect to a single reference frame. A homogenous transformation matrix was used to rotate and translate the coordinates of each Haversian canal based on the position of their corresponding datum points. Once complete, the Haversian coordinates were separated into two separate groups: those that belonged to the interior surface and those that belonged to the exterior surface.

In order to separate the canals into the two groups, black and white images of the center coordinates were created. The images generated were black with white dots indicating the center of each Haversian canal. The coordinates of each image were then rotated once more so that the interior and exterior surfaces of the rib were parallel to the horizontal axis. Thresholds for the distance along the y-axis were then established. Using the threshold specified for each rib section, the canals were divided into the interior and exterior surfaces based on their individual y-coordinate.

In order to determine which coordinates belonged to a single Haversian canal, an algorithm was used to compare the center coordinates from one image to those of the next, representing 300 microns of travel along the rib section. If the coordinates of one canal were within the established limits of a canal in the next image, these coordinates were paired together. The limits were set high enough so that the total travel of the canal between sections could be as high as 20 degrees. Based on previous research this upper limit would ensure that the algorithm would not incorrectly eliminate any canal coordinates. If more than one set of coordinates were paired together the algorithm chose the closest set of coordinates as the correct match.

Once paired coordinates were created from each section throughout the rib specimen, the Haversian canal angles were determined. Since the images had been rotated so that the interior and exterior surfaces were horizontal, changes in the x-coordinate of the Haversian canal directly indicated its motion with respect to the rib axis in the vertical plane. Canal translation to the left in the histological image indicated superior translation in the rib section. The angle of each canal between successive sections was determined by

first dividing the displacement in the x-direction by the distance between histological sections (300μm), then taking the inverse tangent of this value (Figure 3).

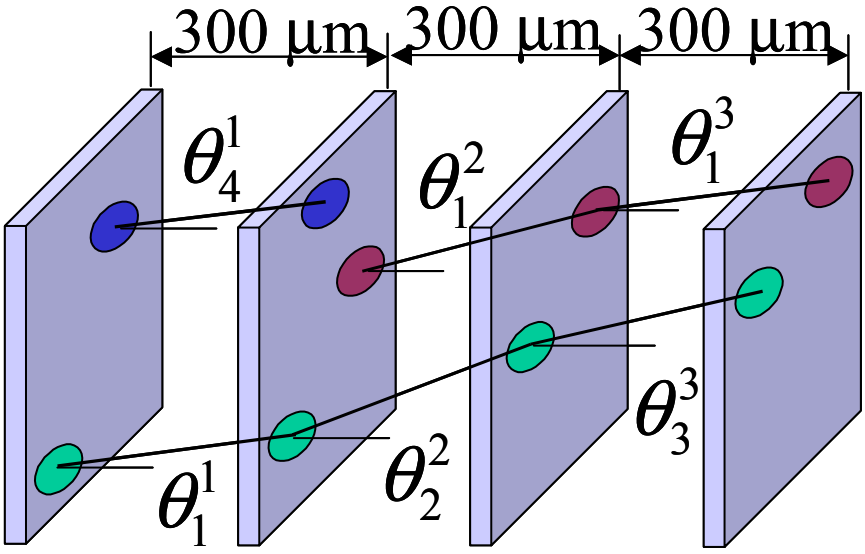

Figure 3:Diagram showing the translation of three separate Haversian canals through 4 histological sections and the determination of the average offset angle.

$$\theta_{section}^{j} = \frac{\sum \theta_i^j}{n_i} \qquad \text{Equation (1)}$$

$$\theta_{average} = \frac{\sum \theta_{section}^{j}}{n_j} \qquad \text{Equation (2)}$$

The Haversian canal offset angle ($\theta_{section}^{j}$) is calculated by taking the average offset angle for all canals between only two histological sections (Equation 1). The variable j represents the histological sections that are being considered for the calculation of $\theta_{section}^{j}$. The offset angle of each Haversian canal is represented by θ_i and n_i is the total number of Haversian angles calculated. The average offset angle of all canals in the entire rib section

($\theta_{average}$) is then calculated (Equation 2).. For this calculation, n_j represents the total number of histological sections created from the rib at the corresponding location.

Results

The average offset angle of osteons in the human rib was determined for various locations from two cadaver subjects (Tables 1-2). The average absolute offset angle for both subjects at all locations was 3.1 degrees, with respect to the rib axis. The average absolute offset angle was 3.15 degrees for the female and 3.03 degrees for the male subjects. The highest offset angles were found in the anterior region of the thorax, with angles of -14.83 and 8.24 degrees for the exterior and interior surfaces respectively. The magnitude of the osteon offset angles in the anterior specimens was found to be significantly higher than those from the posterior locations (p=0.02). The magnitude of the osteon offset angles in the lateral specimens were also found to be significantly higher than those from the posterior locations (p=0.01).

Table 1: Microstructure results from female subject.

Haversian Canal Offset Angle (deg)						
	Interior Surface			External Surface		
Rib	Anterior	Lateral	Posterior	Anterior	Lateral	Posterior
2	-1.864			0.692		
3	2.879	2.875		2.556	1.507	
4	-3.310	-3.517	1.294	-11.390	-8.344	-0.819
5	-6.512	4.611	-0.670	3.472	8.557	-0.912
6		4.578		-14.827	0.914	
7	-1.610	3.917	-1.984	-4.699		0.023
8		0.560	0.078		2.271	-3.011
9		1.004			0.034	
10		0.694			2.833	
11			3.144			2.810
12			3.624			1.186

Table 2: Microstructure results from male subject.

Haversian Canal Offset Angle (deg)						
	Internal Surface			External Surface		
Rib	Anterior	Lateral	Posterior	Anterior	Lateral	Posterior
2		1.52			0.85	
3	-1.12	-3.06		2.43	1.54	
4	-1.91	-6.09	2.49	-0.21	-2.38	4.29
5	8.24	-1.95	4.10	-10.17	5.53	0.31
6	0.46	2.27		-5.42	-7.23	
7	-1.05	7.47	-2.02	1.13	-7.04	1.98
8		0.03			-1.07	
9		4.70			0.61	
10		-3.10			-2.33	
11			0.42			-2.52

Discussion

The results from the histological analysis of human rib specimens showed a variability in osteon direction with respect to the rib axis, but overall trends were evident. This is similar to results obtained by Cohen (1958) who also found a variation in osteon orientation, while still demonstrating an overall pattern of preferred direction. In this study, the short rib lengths analyzed creates difficulties in defining trends within each specimen, however, the average orientation within these specimens does reveal trends within the thorax as a whole.

The average offset angle in both surfaces was highest in the anterior region, then decreased in the lateral region and was lowest in the posterior region. This may reflect the anatomy of the sternal and vertebral attachments with the ends of the rib. The costal cartilage attachments at the sternal end of each rib presents a very rigid joint. In contrast, the vertebral end of each rib is attached via ligaments, 7 for the second through tenth ribs and 3 ligaments for the remaining three ribs. These joints allow more movement of the rib

to facilitate respiration and therefore may alter the loading conditions seen at the anterior and posterior portions of each rib. These different loading conditions may alter the way in which the bone adapts due to differences in the forces that the rib is exposed to at the vertebral and sternal joints. This may explain the statistically significant differences among the anterior, lateral and posterior osteon offset angles.

Helical patterns similar to those found by previous research were also observed at all location of some ribs and at different locations of others. For example, the seventh rib from the male subject exhibited almost opposite offset angles between the interior and exterior surfaces at the anterior, lateral and posterior locations. This would create the crisscross pattern expected between the interior and exterior surface osteons to create the helical pattern. This pattern was seen in other ribs to a varying degree as well, which is consistent to findings in previous research on the human femur (Hert 1994).

Variations among the offset angles determined during this study may be due to the short length of rib sections analyzed. Shorter specimens were used in order to produce results for each rib, rather than only a few select ribs. The computer algorithms developed in this study facilitates the analysis of a large number of samples due to the automation it provides. Future studies may want to consider only one or two ribs so that a map of the osteons for the entire rib may be generated.

Conclusions

Previous research has shown that the strongest direction of cortical bone is determined by osteon orientation. Therefore, knowing the orientation of osteons in the human rib cage may provide insight into the adaptation processes of bone. The orientation

of osteons in the human rib may also explain any anisotropic behavior seen in individual ribs as well as variations in the strength of a single rib along its length.

The osteon orientation in the human rib cage was investigated using a total of 74 rib specimens removed from two cadavers. A total of 152 and 162 images of histological slides were created from a female and male subject respectively. The location of osteons in the interior and exterior surface of each rib was determined by digitally analyzing histological images using algorithms written in Matlab. An average absolute offset angle for both subjects was found to be 3.1 degrees with respect to the rib axis for all specimens.

The average offset angle of osteons with respect to the rib axis was significantly different between specimens removed from anterior, lateral and posterior locations of the rib cage ($P=0.01$). Osteons in the posterior specimens displayed the lowest offset angle, with an average of 1.8 degrees with respect to the rib axis. The lateral and anterior locations showed increasing average offset angles of 3.2 and 4.1 degrees respectively. Differences in osteon orientation along a single rib may reflect the influence of anatomy of the rib joints at the sternum and vertebral bodies.

The quantification of osteon orientation in the human rib cage provided by the current study, contributes to the present understanding of rib anisotropic behavior and bone adaptation. This study represents a first step in determining the orientation of osteons in the rib cage and describes a methodology that can be applied to any histological analysis of bone. This knowledge can be used to expand current models used to predict thoracic trauma.

References

Black J, Richardson SP, Mattson RU, Pollack SR: Haversian Osteons: Longitudinal Variation of Internal Structure. J Biomed. Mat. Res., 14: 41-53; 1980.

Carter D.R.: Mechanical Loading Histories and Cortical Bone Remodeling. *Calcif. Tissue Int.,* 36: S19-S24; 1984.

Cohen J, Harris WH: The Three-Dimensional Anatomy of the haversian System. J. Bone Joint Surg., 40A: 419-434; 1958.

Cowin S.C.: Wolff's Law of Trabecular Architecture at Remodeling Equilibrium. *J. Biomech. Eng.,* 108: 83-88; 1986.

Hayes W.C., Swenson L.W., Schurman D.J.: Axisymmetric Finite Element Analysis of the Lateral Tibial Plateau. *J. Biomech.,* 11: 21-22; 1978.

Hert J, Fiala P, Petrtyl M: Osteon Orientation of the Diaphysis of the Long Bones in Man. Bone, 15(3): 269-277; 1994.

Lanyon L.E., Bourn S.: The Influence of Mechanical Function on the Development and Remodeling of the Tibia. *J. Bone J. Surg.,* 61A: 263-272; 1979.

Martin R.B., Burr D.B.: Structure, Function and Adaptation of Compact Bone. New York: Raven Press; 1989.

Martin R.B.: A Theory of Fatigue Damage Accumulation and Repair in Cortical Bone. *J. Orthopaed. Res.,* 10: 818-825; 1992.

Petrtỳl M.: Reactivities of the Compact Femoral Bone to the External Load. *Proceedings of the 24th Congress of Biomech.,* Paris: 1028-1029; 1993.

Petrtỳl M.: Spiral Flow of Elastic Properties in the Compact Femoral Bone. *Proceedings of the 25th Congress of Eur. Soc. Artif. Organs,* Prague: 141-145; 1988.

Rubin C.T. Housman M.R.: The Cellular Basis of Wolff's Law. Transduction of Physical Stimuli to Skeletal Adaptation. *Rheum. Dis. Clin. North. Am.,* 14: 502-517; 1988.

Wolff J.: *Das Gesetz der Transformation der Knochen.* Berlin: Hirschwald; 1892.

CHAPTER 3

The Mechanical Characterization of Human Ribs Subjected to Dynamic Three-Point Bending

Abstract

Determining the risk of injury from an automobile collision to the thorax requires knowledge of the properties of the skeletal components that comprise the thorax. The purpose of this study was to investigate the strength of human ribs subjected to dynamic three-point bending. A total of four human cadavers were utilized by removing 16 rib sections from the right side of each thorax. One or two sections were removed from a single rib at the lateral, anterior and posterior locations of the thorax. The strain rates resulting from the dynamic loading ranged from 0.5 to 5.44 strains per second. Three-axis strain gage rosettes were used for one series of tests showing small variation of the principal strain axis from the direction of bending. For all subjects, the anterior specimens failed at a significantly lower peak stress than the lateral ($p=0.01$) and posterior ($p=0.01$) specimens. The average elastic modulus from all tests was 22 GPa. The average peak stress for all specimens was 115 MPa, with an average peak strain of 11,460 microstrain.

Introduction

Human ribs play an important role in the protection of vital organs essential to the life of an individual. In order to properly predict forces that will initiate rib fracture, the strength of each rib should be investigated. The rib response to dynamic loading is of particular interest for the development of injury criteria applied to automotive safety devices. Studies using restrained cadavers in impact sled tests have frequently found rib fracture to be the most common skeletal injury (Crandall 1997, Kallieris 1998, Cromack

1975, Patrick 1974, Ramet 1979). This study is an improvement to previous work due to the use of dynamic loading as well as the use of ribs from a wider range of locations on the thorax.

Previous work on human ribs includes non-destructive tests performed by Shultz *et al.* (1974). These tests were performed using a cantilever end condition and resulted in force-displacement data showing no difference in stiffness among the ribs tested at different levels of the thorax. These included the second, fourth, sixth and the eighth through the tenth ribs. The use of a cantilever end condition is not an accurate way to recreate rib loading observed *in vivo,* however, this study provides useful information for model validation. Granik and Stein (1973) performed static three-point bending tests on lateral rib sections from the 6^{th} and 7^{th} ribs. For the ten cadavers tested, loading in the lateral/medial direction resulted in an average failure stress of 106 MPa and an average Young's modulus of 11.5 GPa. Stein and Granik (1976) performed static three-point bending tests on a total of 79 male cadaver subjects, utilizing the 6^{th} and 7^{th} ribs from each. Quasistatic loading was performed in the medial/lateral direction at rates of 2.54, 0.508 and 12.7 mm/min. The average failure stress for all tests was 100.68 MPa, with a variance of 19% of the mean.

More recently, Yoganandan and Pintar (1998) performed quasistatic three-point bending tests on the 7^{th} and 8^{th} ribs of 30 subjects. The authors found no significant difference between the strength parameter for the two ribs. An average Young's modulus of 2318 MPa for the seventh rib and 1886 MPa for the eighth rib was determined. The average force at fracture was 153 and 137 N for the seventh and eight rib. Other studies include those consisting of geometric measurements as well as chest compression

measurements on human volunteers (Jordanoglou 1969, Roberts 1972, Wilson 1987). Studies like these are important for a global understanding of the thorax. However, in order to produce a more accurate representation, more localized properties need to be determined.

Knowledge of impact tolerances for biological tissue is essential in the development of injury risk analyses. The purpose of this study was to determine the response of human ribs to dynamic three-point bending. The use of a wide range of rib specimens for this study is hoped to increase the knowledge of the human rib response to dynamic loading.

Methodology

A total of 59 rib specimens were removed from four cadaver subjects. A total of 16 test specimens were removed from ribs 2 through 12 on the right side of the thorax (Figure 1). In two instances, the 11^{th} and 12^{th} ribs had been removed before obtaining the subject for the current study. Therefore, in the case of the male subjects, these rib specimens were not available for analysis. The length of each specimen was determined by the longest section that could be removed and still produce a usable section. The lower ribs were more consistent in there geometry and, therefore, specimens of similar lengths could be prepared from these ribs. The ribs were removed using an autopsy saw and were wrapped in saline soaked gauze and stored in an air-tight container. The periosteum was left intact to yield an accurate representation of rib strength and to mitigate bone deterioration.

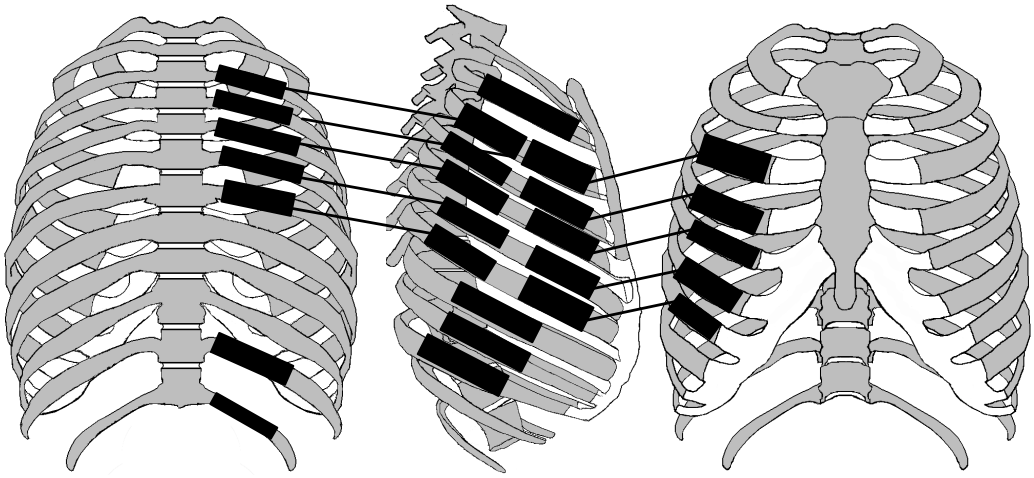

Figure 1: Location of rib specimens used for dynamic three-point bending analysis (posterior view on left, lateral and anterior at right; connecting lines represent same specimen).

The bone mineral density of the cadaver subjects was determined by using the Osteogram® technique (Osteogram®, San Diego, CA) (Table 1). This procedure uses radiographs of the subject's hand and forearm with a phantom for calibration. The radiograph is then scanned and the bone mineral density is determined and presented as an Osteogram® bone mineral density index, or BMD Index. The BMD Index is not the actual bone mineral density, but rather an index number relative to other Osteogram® scans. More useful outputs from this technique are the BMD T-score, and BMD Z-score. The BMD T-score represents the number of standard deviations away from the average the subject's bone mineral content is compared to the average healthy individual between 25 and 50 years. The positive or negative T-score value denotes greater or lower bone mineral density respectively. T- scores at -1.0 or greater are considered normal, between -2.5 and -1.0 indicates a low bone mineral density, and below -3.0 is considered osteoporotic. The Z-score is the number of standard deviations away from the average bone mineral density

of females at the subject's age. The Z-score is particularly important for females due to the decrease in bone mineral density after menopause and, therefore, is not reported for males.

Table 1: Cadaver data for specimens used during current work.

Cadaver Number	Gender	Age	BMD Index	T-score	Z-score
M1	Male	71	90.3	-1.9	N/A
F1	Female	61	77.9	-3.0	-1.2
M2	Male	61	83.2	-2.5	N/A
F2	Female	67	75.2	-3.3	-1.0

All tests were performed in the appropriate bending direction in order to simulate frontal loading of the thorax. The rib specimens removed from the anterior region of the thorax were loaded in the anterior-posterior direction. This placed the interior surface of the rib in tension, which would be expected when the thorax is exposed to seat belt loading during an automobile collision (Yoganandan 1991, 1993). The lateral rib specimens were loaded in the medial-lateral direction, which placed the exterior surface of these specimens in tension. This loading state at the lateral region of the thorax is due to the compression of the thorax in the anterior-posterior direction during a frontal impact. Finally, the posterior rib specimens were loaded in the posterior-anterior direction, creating tensile forces on the internal surface of the rib specimen. This loading condition was shown in anterior-posterior compression of cadaver and case study investigations (Yoganandan 1991,1993, Kleinman 1997).

Before testing, a strain gage (Model CEA06062UW350, Vishay Measurements Group, Raleigh NC) was attached to the surface of the rib that would be exposed to tensile strain. An area of periosteum, slightly larger than the strain gage was removed from the central region of each rib. The strain gage was positioned in the middle of the rib span and attached using the manufacturer's suggested procedure (Figure 2). Latex gloves were worn

during the application of the strain gage, as well as an extra thumb cut-out over the thumb used to apply pressure to the gage. This extra thumb remained on the rib after application.

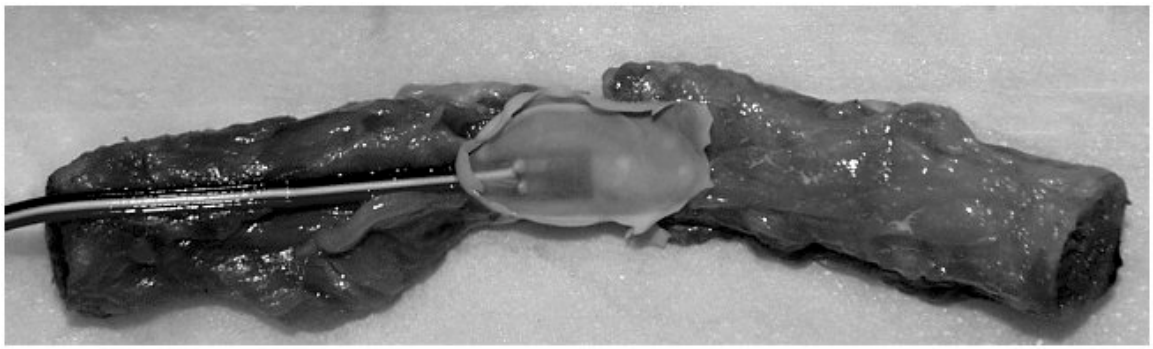

Figure 2: Rib specimen instrumented with a strain gage ready for testing.

Initial testing was performed using rib sections from one cadaver instrumented with a rectangular stain gage rosette. The center gage was oriented parallel to the rib axis at the center of the rib. The remaining two gages were offset 45 degrees from the center gage in either direction. Initial data using the stain gage rosettes was used to determine the orientation and magnitude of the principal strain in each rib during dynamic bending. The initial tests revealed that the principal strain direction deviated an insignificant amount from the axis of the rib and, therefore, the remaining tests were performed using a single axis strain gage configuration.

An MTS (Model 810, MTS, Raleigh, NC) servohydraulic test machine was used to apply the dynamic loading to the rib specimens. A specially designed apparatus was machined from 2051 aluminum to securely support the rib section (Figure 3). A load cell was attached to the impacting blade of the device to measure the load imposed on the rib specimen during the event (Model 1210AF, Interface, Scottsdale AZ). The MTS machine was equipped with a Microcontroller (Model 458, MTS, Raleigh, NC) and Microprofiler (Model 418.91, MTS, Raleigh, NC) that delivered the loading signal causing an average

displacement rate of 500-1000 mm/sec. An Iotech Wavebook data acquisition system (Wavebook 516, Iotech, Cleveland, OH) was used to record data during the event at 10kHz. The motion occurring during each test was also recorded using high speed digital video (Phantom 5, Vision Research, Wayne, NJ) at 1000 fps.

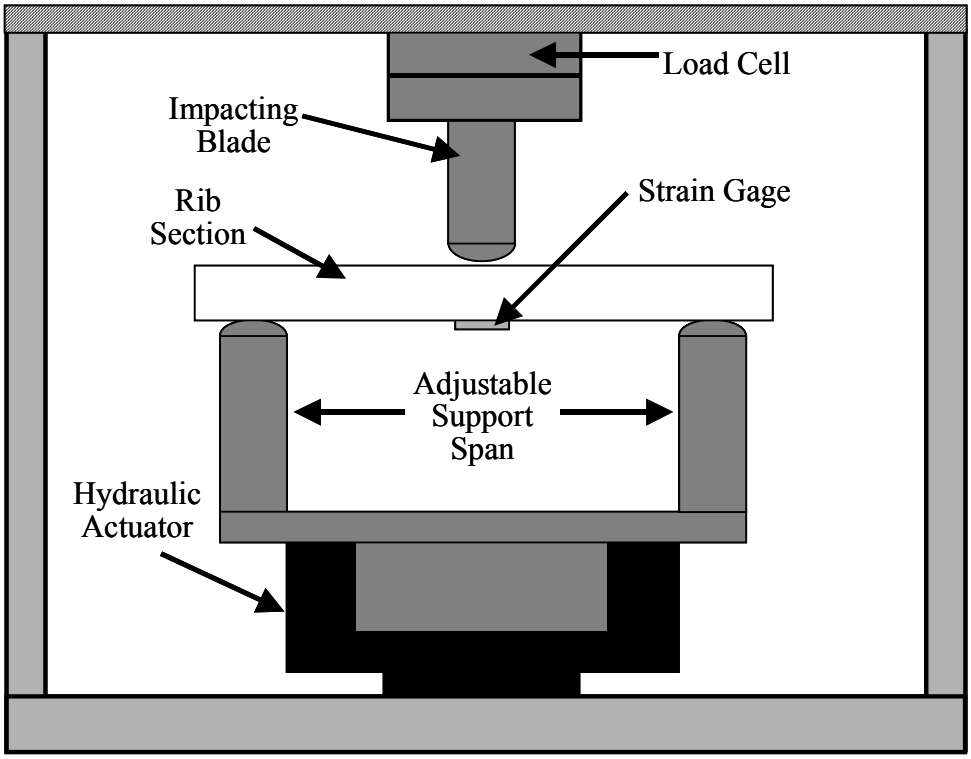

Figure 3: Apparatus used to evaluate human rib response to dynamic three-point bending.

Cross sectional area of the ribs was determined from gross measurements and digitized photography after testing. The cross sectional area of the rib at the location of fracture was determined by making a perpendicular cut across the rib near the fracture (Figure 4). A digital image of the rib cross section was then analyzed using a computer algorithm to determine the second area moment about the superior/inferior axis of the rib. With force and displacement data, the failure stress was determined.

Figure 4: Geometric data gathered from rib specimen cross section for stress calculation.

Results

A total of 59 rib section tests were performed in dynamic three-point bending. Geometric data was used to determine peak stresses as well as the elastic modulus of each rib. Strain data from the tests performed using strain gage rosettes facilitated the calculation of the principal strain magnitude and direction (Figure 5). The strain measured by the axial gage (Gage 2) coincided with the principal strain determined using the other 2 strain gage measurements. The principal angle also showed little deviation from the longitudinal direction of the rib. The average principal angle at failure was 3.7 degrees for all specimens. The average angle for the individual regions was 4.54 for the anterior, 4.43 for the lateral and 2.67 for the posterior rib specimens. These results suggest that the use of axial strain gages in the remaining tests sufficed for accurate stain measurement.

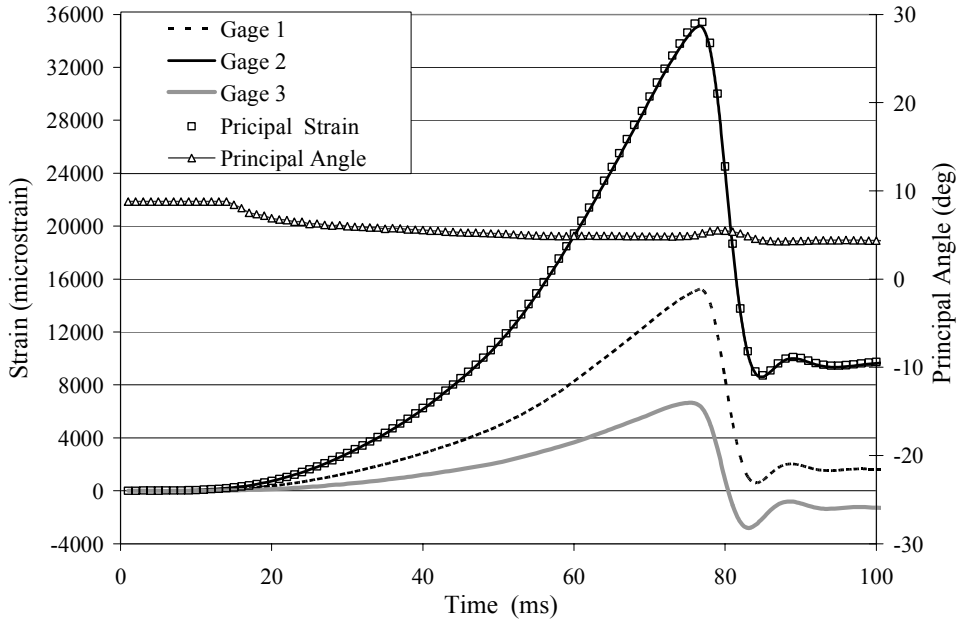

Figure 5: Strain and principal strain composition recorded during rib bending test with rectangular strain gage rosette.

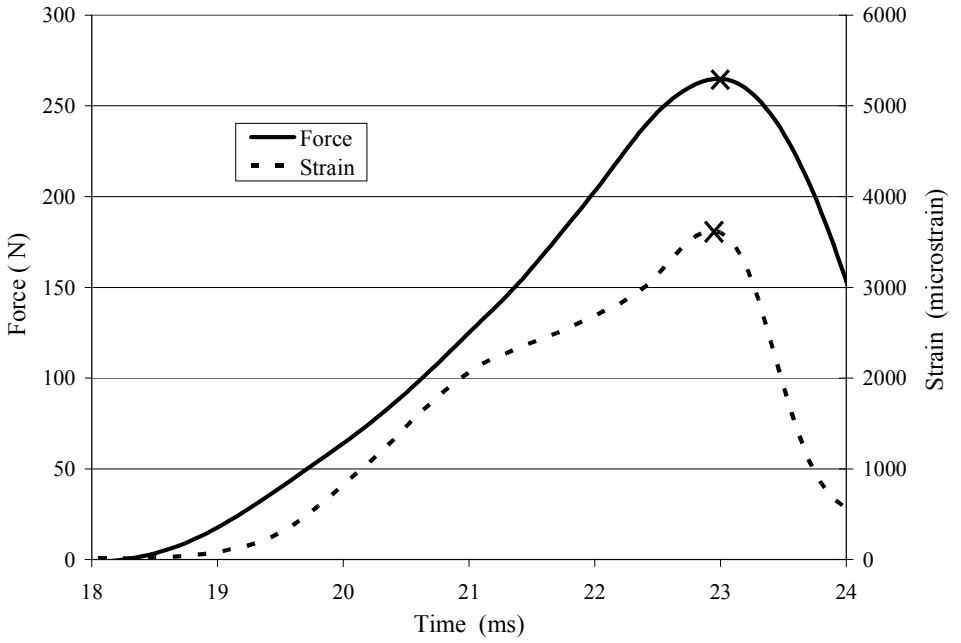

Figure 6: Force and strain trace recorded during dynamic three-point bending using axial strain gage only.

The strain rates resulting from the dynamic loading were calculated from strain versus time plots and their values ranged from 0.5 to 5.44 strains per second (Figure 6). The average strain rate for each series of tests performed on a single cadaver is listed with the corresponding data (Tables 2-5). The A, L and P notation for the rib specimens indicates the anterior, lateral and posterior regions of the rib. The number before the region letter indicates from which rib the specimen was removed. As a result of rib size or geometry, there were five instances in which a rib specimen could not be tested. These were: F1-03A, F2-06P, F2-07P, M1-04A and M1-03A.

The average elastic modulus of the rib specimens for all subjects was 22.46 GPa for the anterior, 23.29 GPa for the lateral and 19.95 GPa for the posterior regions. The average peak stress for all subjects was 78.33 MPa, 126.96 MPa and 135.81 MPa for the anterior, lateral and posterior locations respectively. Student two-tailed t-tests were performed assuming unequal variances to identify statistically significant differences between the peak strain, peak stress, elastic modulus and moment of inertia values obtained during the study.

Table 2: Results for cadaver F1 with an average strain rate of 2.27 strains/s and standard deviation of 1.32 (με = microstrain).

Rib Specimen	Peak Force (N)	Peak Strain (με)	Span (cm)	Ixx (mm^4)	Peak Stress (MPa)	Elastic Modulus (MPa)
02L	46	16500	5.40	14.68	71.24	16.62
03P	96	7248	5.65	27.23	109.94	18.97
04A	39	3211	7.48	30.47	48.32	18.92
04P	112	6571	6.66	70.44	80.43	16.10
05A	65	5967	7.48	31.80	74.57	19.70
05P	185	12324	5.65	62.27	126.23	19.86
06A	81	7082	6.48	35.95	78.90	12.46
06P	175	21658	6.66	37.56	168.09	16.88
07A	65	4201	6.48	38.17	59.25	20.93
07P	187	21051	6.66	39.17	175.69	16.86
08L	67	8002	9.11	36.45	90.79	14.72
09L	77	8373	7.91	38.06	94.95	31.39
10L	68	6995	7.45	23.18	112.91	45.34
11P	79	18621	7.51	16.58	144.65	14.68
12P	67	11688	5.60	20.99	73.82	11.37

Table 3: Results for cadaver F2 with an average strain rate of 3.62 strains/s and standard deviation of 1.41.

Rib Specimen	Peak Force (N)	Peak Strain (με)	Span (cm)	Ixx (mm^4)	Peak Stress (MPa)	Elastic Modulus (MPa)
02L	98	10505	6.46	46.48	77.50	15.95
03A	130	4029	5.94	48.26	111.57	86.81
03P	161	18026	5.52	35.16	138.09	26.22
04A	108	4400	5.94	80.27	49.28	11.68
04P	241	11518	5.52	77.57	137.21	13.58
05A	167	5756	5.52	128.99	55.14	13.07
05P	265	3629	6.74	110.63	130.92	36.88
06A	100	3724	5.94	75.23	54.99	11.43
07A	169	6501	5.94	102.40	67.16	12.10
08L	176	12937	8.20	67.24	148.10	28.89
09L	203	8876	8.20	80.00	133.45	20.57
10L	215	35023	8.20	66.39	161.59	19.10
11P	212	28396	6.74	44.57	167.78	18.06
12P	85	8167	5.44	18.87	94.99	23.36

Table 4: Results for cadaver M1 with an average strain rate of 1.53 strains/s and standard deviation of 0.60.

Rib Specimen	Peak Force (N)	Peak Strain (με)	Span (cm)	Ixx (mm^4)	Peak Stress (MPa)	Elastic Modulus (MPa)
02L	104	4909	8.37	65.27	79.01	42.93
03A	166	8588	6.33	57.76	135.98	24.92
03P	221	20168	6.11	78.24	132.22	6.52
04P	177	3112	8.89	61.54	171.57	62.50
05A	155	4875	7.26	94.42	85.63	21.24
05P	203	10880	9.23	123.13	135.61	12.92
06A	249	10846	8.20	118.75	134.75	14.58
06P	330	10949	8.20	160.56	160.14	11.31
07A	243	12947	8.20	93.70	164.66	53.51
07P	327	24671	8.20	140.89	156.30	35.72
08L	239	18348	10.59	79.91	200.31	31.59
09L	188	18060	10.59	66.24	183.45	25.57
10L	199	15651	8.85	68.49	195.54	11.47

Table 5: Results for cadaver M2 with an average strain rate of 1.67 strains/s and standard deviation of 0.55.

Rib Specimen	Peak Force (N)	Peak Strain (με)	Span (cm)	Ixx (mm^4)	Peak Stress (MPa)	Elastic Modulus (MPa)
02L	93	5469	6.82	84.60	54.34	10.70
03P	291	11950	5.73	108.08	152.73	17.15
04A	56	6288	6.44	84.45	32.82	21.90
04P	328	16081	6.44	121.01	191.82	16.34
05A	86	6087	7.42	84.85	56.57	14.95
05P	221	8571	6.44	118.10	109.94	15.48
06A	122	5366	7.42	126.17	52.13	11.02
06P	344	21416	7.52	230.67	117.50	13.15
07A	118	8042	7.42	86.18	69.85	12.63
07P	272	12940	7.52	175.10	112.23	14.88
08L	151	9925	9.97	91.77	111.48	15.70
09L	213	12371	7.43	71.51	138.69	19.97
10L	199	20706	6.49	42.04	177.98	22.17

There are several different means of grouping the data collected from the current study in order to perform statistical analyses. The first approach was to group all the data for both genders and compare by the region from which the specimens were removed. This revealed that the average peak strain in all the anterior specimens was significantly lower than both the lateral (P=0.01) and posterior (P=0.01) specimens. The average peak stress values showed the same relationship in that they were significantly lower for the anterior specimens when compared to lateral (P=0.01) and posterior (P=0.01) specimens. The moment of inertia of the anterior specimens was lower than the lateral specimens, on the average (P=0.07), however, the difference was not statistically significant. The average moment of inertia of the lateral specimens was lower than the average posterior values for all specimens (P=0.06), but again, the difference was not statistically significant.

Grouping all data from all regions between the two genders resulted in only one significant difference. The difference in the moment of inertia of all male and female rib specimens was the only variable found to be statistically significant (P=0.01) at this level of grouping. Female moment of inertia values were significantly lower than that of the male subjects. The peak stress for all the female specimens, was lower on the average when compared to the male specimens, but fell short of being statistically significant (P=0.07).

Dividing the rib specimen data between genders revealed more significant differences in the anterior, lateral and posterior regions among the two genders. These comparisons were performed by focusing on one location and comparing between the two genders. Among the anterior specimens, the average peak strain for the female subjects was significantly lower than the male anterior specimens (P=0.01). The average moment of inertia of the female specimens was significantly lower at all three locations, the anterior

(P=0.05), lateral (P=0.01) and posterior specimens (P=0.01) when compared to those of the male subjects at the corresponding locations.

The next grouping scheme only considers the specimens for the female subjects and comparisons are made between each location. The peak strain in the anterior specimens was significantly lower than in the lateral (P=0.01) and posterior (P=0.01) specimens at fracture. This same pattern holds for the peak stress values as well, showing a significantly lower peak stress for the anterior specimens when compared to the lateral (P=0.01) and posterior (P=0.01) specimens. The were no statistically significant difference between the moment of inertia values among rib specimens from the various locations.

Grouping the male data only and comparing between specimen locations generated similar patterns as seen in the female specimens. The peak strain measured in the anterior specimens was significantly lower than those of the lateral (P=0.01) and posterior (P=0.01) sections. The peak stress values for the anterior specimens were also significantly lower than the values measured in the posterior (P=0.01) specimens. The moment of inertia values for the male specimens did show statistically significant differences. The lateral specimens had a significantly lower moment of inertia value than the anterior (P=0.01) and posterior (P=0.01) specimens. The moment of inertia of the anterior specimens was significantly lower than the posterior (P=0.01) specimens.

Comparisons were made between all specimens tested from the individual cadaver subject as well as specimens from each region. The peak stress values from all locations of the M2 male subject were significantly higher than the F1 female subject, (P=0.01) the F2 female subject (P=0.02) and the M2 male subject (P=0.02). The anterior specimens from the M2 male subject demonstrated a higher peak stress than those from the same location of

the F1 female (P=0.01) and F2 female subjects (P=0.01). Grouping all moment of inertia values for each subject revealed the F1 female subject had significantly lower values than the F2 female (P=0.01), the M1 male (P=0.01) and the M2 male subjects (P=0.01). The 2F female subject also had significantly lower moment of inertia values for all specimens tested than the 2M male subject (P=0.02). Grouping the moment of inertia values into the anterior region only, showed the F1 female subject to have a significantly lower value than F2 female (P=0.02), M1 male (P=0.02) and M2 male subject (P=0.01). The lateral specimens displayed the same trends for moment of inertia with the F1 female subject having significantly lower values than the F2 female (P=0.01), M1 male (P=0.01) and M2 male subject (P=0.02). Considering the moment of inertia values for the posterior specimens revealed the F1 female subject to have significantly lower values than both the M1 male (P=0.01) and M2 male subject (P=0.01). The same was true for the F2 female subject which had significantly lower moment of inertia values than the M1 male (P=0.05) and M2 male subject (P=0.01).

The final grouping by subjects considered the peak force values measured in the specimens during the dynamic three-point bending analysis. The peak force for all specimens from the F1 female subject was significantly lower than those of the F1 female, (P=0.01) M1 male, (P=0.01) and M2 male subject (P=0.01). Grouping the peak force values for the anterior region revealed significantly lower values for the F1 female subject than the F2 female (P=0.01) and M1 male subject (P=0.01). The 1M male subject also had a significantly lower peak stress than the M2 male subject (P=0.01). The lateral specimens demonstrated the same trends, with the F1 female subject having a significantly lower peak force than the F2 female ,(P=0.03) M1 male (P=0.03) and M2 male subject (P=0.04). The

posterior region is finally compared, indicated that these specimens from F1 female subject had significantly lower peak force values than the M1 male (P=0.01) and M2 male subject (P=0.01).

Discussion

The results of this investigation on the response of human ribs to dynamic three-point bending suggest that there are differences in rib properties at different locations in the thorax. These differences can be attributed to variations in geometry and microstructural properties between ribs and along each rib in the thorax. The posterior ribs for example, failed at a significantly higher stress than the anterior specimens (p=0.01) and also had the significantly highest moment of inertia (p=0.04). There was no significant differences among the moment of inertia values for the female subjects. However, the female moment of inertia values were significantly lower than those of the males (P=0.01). These comparisons were made by grouping the specimens together for all subjects. There were differences between the subjects themselves, which contributed to the differences described above.

Grouping the specimens by each subject allows for comparisons to be made by age and in this case, the importance of BMD data was highlighted. The F1 female subject was given the second lowest BMD score (T=-3) and exhibited the lowest peak force and moment of inertia values when compared by body region and the combined data for all specimens. The F2 female subject had the lowest BMD score (T=-3.3) but combining the specimens together was the comparison that showed significant differences between peak force and moment of inertia values. The posterior specimens were the exception, however, which had lower moment of inertia values for the F2 female than the two male subjects.

The two male BMD scores were similar, however the M2 male had a lower score (T=-2.5). This may be responsible for the lower overall peak stress and elastic modulus than the M1 male subject (T=-1.9). The fact that the results for the male subject correlated with BMD may suggest better adaptability with age, or because there score were not substantially low, osteoporosis is not a factor. These result show that age is not the only factor when considering the strength of the thorax. The M2 male was younger than the M1 male, but because of the lower BMD, the M2's mechanical characteristics had diminished to a greater extent.

The fact that the anterior region of the thorax failed at a lower stress overall is supported by impact sled tests that have been performed on restrained cadaver occupants. In most cases the rib fractures that occurred were isolated to the anterior portion of the rib cage (Kallieris 1982, Schmidt 1974, Yoganandan 1991, 1993). This may be an effect of the loading provided by the shoulder belt during the crash, however, the current study suggests that it may also be due to the strength of the rib cage at this region exposed to the shoulder belt. Nevertheless, it is an important consideration when attempting to develop a predictive tool for thoracic injury during an automobile collision.

The mechanical properties of human ribs determined during this investigation are in accord with previous work on static rib bending. The elastic modulus values obtained in this study were higher, however this was expected due to the utilization of higher loading rates. Yoganandan and Pintar (1998) reported elastic modulus values of 2.3 GPa and 1.9 GPa for the seventh and eight ribs respectively. These values were obtained from a loading rate of 2.5 mm/min. The average elastic modulus calculated during this investigation for the eighth, ninth and tenth lateral specimens was 24 GPa at loading rates of 500-1000 mm/s.

These ribs were chosen for comparison in order to match the loading directions used by Yoganandan and Pintar (1998). The difference in elastic moduli between previous work and the current work exemplifies the importance of dynamic analysis of biological tissue.

The effects of rib curvature on the strength of the rib were found to be minimal. The change in stress values in a curved beam is a function of its radius of curvature (R) and its depth (d) in the plane of bending. These parameters were investigated for the F1 female subject and similar geometry was assumed to be present in the other subjects. This is a reasonable assumption because the male subjects were larger so one would expect the radius of curvature to increase. Therefore, the F1 subject represents the worst case for the effects of rib curvature. The ratio R/d defines the significance of the curvature of a beam and was determined for all specimens removed from the F1 subject. An R/d value of 8 represents the limit to which straight-beam theory applies with minimal errors that are on the order of 4% to 5% (Young 1989). The average depth for all subjects was: 0.17 in. for subject F1, .20 in. for subject F2, 0.24 in. for subjects M1 and 0.26 in. for subject M2. The average radius of curvature (R) for the F1 subject was 6.28 inches. The average of the R/d values for the F1 subject was 38, therefore the influence of rib curvature was assumed to be negligible for all subjects because of similar geometry.

An interesting finding during this investigation was the strength of the periosteum surrounding the ribs. In many of the rib fracture tests, the cortical bone would fail corresponding to a drop in the load, but the periosteum would continue to provide structural stability to the rib around the fracture location. This finding indicates that a more detailed analysis of the periosteum should be considered.

Conclusions

The purpose of this study was to investigate the response of human ribs to dynamic three-point bending. The results of this study using 59 human rib specimens suggest that there is variation in rib strength between the anterior and posterior regions of the rib cage. The anterior specimens were significantly weaker than the posterior in both female ($p=0.01$) and male ($p=0.01$) subjects. The peak strain measured from the anterior specimen tests were significantly lower than those of the lateral ($P=0.01$) and posterior ($P=0.01$) sections. This pattern was true among both genders. There were no significant differences between peak stress values for rib specimens removed from male and female subjects. The elastic modulus measured from stress strain curves ranged from 19.95 GPa to 23.29 GPa on average, which is a significant increase over values obtained during previous quasistatic bending studies. This was expected because of the viscoelastic behavior of biological tissues.

The information obtained in this study is an addition to current knowledge of the dynamic properties of human ribs. The use of dynamic loading rates is of particular importance for the prediction of injuries incurred during an automobile collision. The results of the current study reinforce trends in rib fracture locations observed in impact sled tests performed using belting cadaver occupants. These studies showed that the anterior region of the thorax, which was determined to be the weakest region in the current work, has the highest occurrence of fractures. Overall, the current work suggests that variations in rib strength are present among regions of the thorax. Therefore, to produce an improved model for the prediction of thoracic injury, these differences in mechanical characteristics need to be accounted for.

References

Crandall JR, Bass CR, Pilkey WD, Miller HJ, Sikorski J, Wilkins M: Thoracic Response and Injury with Belt, Driver Side Airbag and Force Limited Belt Restraint Systems. International Journal of Crashworthiness, 2(1): 119-132; 1997.

Cromack JR, Ziper HH: Three-Point Belt Induced Injuries: A Comparison Between Laboratory Surrogates and Real World Accident Victoms. Proceedings of the 19th Stapp Car Crash Conference, Society of Automotive Engineers., 751141: 1-22; 1975.

Granik G, Stein I: Human Ribs: Static Testing as a Promising Medical Appplication. J Biomech.,6:237-240; 1973.

Jordanoglou J: Rib Movement in Health, Kyphoscoliosis and Ankylosing Spondylitis, Thorax, 24: 407-14; 1969.

Kallieris D, Zerial PD, Rizzetti A, Mattern R: Prediction of Thoracic Injuries in Frontal Collisions. Enhanced Safety of Vehicles, 98-S7-O-04: 1550-63; 1998.

Kleinman P.K., Schlesinger A.E.: Mechanical Factors Associated with Posterior Rib Fractures: Laboratory and Case Studies. *Pediatr. Radiol.,* 27: 87-91; 1997.

Patrick LM, Anderson A, Bohlin N: Three-Point Harness Accident and Laboratory Data Comparison. Proceedings of the 18th Stapp Car Crash Conference, Society of Automotive Engineers, 741181; 1974.

Ramet M Cesari: Behaviour of Restrained Dummies and Cadavers in Frontal Impacts. IRCOBI: 210-19; 1979.

Roberts SB, Chen PH: Global Geometric Characteristics of Typical Human Ribs. J Biomech., 5: 191-201; 1972.

Schultz AB, Benson DR, Hirsch C: Force-Deformation Properties of Human Ribs. J Biomech., 7: 303-9; 1974.

Sedlin E.D., Frost H.M., Villanueva A.R.: Variations in Cross Sectional Area of Rib Cortex with Age. *J. Geront.,* 18: 19-13; 1963.

Stein ID, Granik G: Rib Structure and Bending: An Autopsy Study. Calcif. Tiss. Res., 20(1): 61-73; 1976.

Takahashi H, Frost HM: Age and Sex Related Changes in the Amount of Cortex of Normal Human Ribs. Acta Orthopead. Scand., 37: 122-30; 1966.

Wilson TA, Rehder S, Krayer Hoffman EA, Whitney CG, Rodarte JR.: Geometry and Respiratory Displacement of Human Ribs. J. Appl. Physiol., 62: 1872-1877; 1987.

Yoganandan N, Skrade D, Pintar FA, Reinartz J, Sances A: Thoracic Deformation Contours in a Frontal Impact. *Proceedings of the 35th Stapp Car Crash Conference, Society of Automotive Engineers,* 912891; 1991.

Yoganandan N, Pintar FA, Skrade D, Chmiel W, Reinartz JM, Sances A: Thoracic Biomechanics with Air Bag Restraint. *Proceedings of the 37th Stapp Car Crash Conference, Society of Automotive Engineers.* 133-144*,* 933121; 1993.

Yoganandan N, Pintar FA: Biomechanics of Human Thoracic Ribs. J Biomech. Eng., 120: 100-4; 1998.

Young W.C: Roark's Formulas for Stress & Strain, 6th Ed. McGraw Hill, Washington D.C.; 1989.

APPENDIX A:

Matlab Algorithms for Histological Analysis

The following Matlab algorithms were used to identify haversian canals located in rib sections removed from various regions of two human thoraces. The general methods that the algorithm applies are described Chapter 2.

```
% This algorithm is the Master file that loads images from
the histological sections
% subroutines are then called up to locate the haversian
canals in each image.

%Load images

%list=char('01A','02A','03A','04A','05A','06A','07A','08A');


%for e=1:length(list)
       % file=sprintf('list.txt',e)
       clear
    clc
    im=imread('08A','tif');
    run local_command

    %end

% This alrogithm is the second in order for determine the
coordinates of the haversian canals in each histological
image
% It makes sure that the area the code is looking at is
actually an enclosed circle, indicating that it has found a
% haversian canal.

%bw = double(im);
bw=im;
%imwrite('bw,sm2702ln01mat,tif')
%image('bw')
[row , col] = size(bw);
coord=ones(size(bw));
area = sum(sum(bw));
limit=30;
oc=0;
lowlimit=1;
```

```
for r=2:row
    %disp('Next Row..')

    for c=2:col
                fail1=0;
                fail2=0;
                fail3=0;

        if (bw(r,c) == 1) & (bw(r,c-1) == 0) &
(bw(r,c+lowlimit) == 1)

            %disp('Engaging White area...')

            run local_sub01

         % Checks for ones above to left, center and right
        if fail1 == 1;
          % ('Moving to Next Column')
         skipcolumn=1;

        else
            skipcolumn=0;
            run local_sub02

        end
         % Creates span of ones and checks for limit

            if fail2 == 1 & skipcolumn == 0
                %disp('Limit Exceeded')

            elseif fail2 ==0 & skipcolumn == 0
                run local_sub03
            end
         % Checks through span for ones
            if fail3 == 1 & skipcolumn == 0
               % disp('Ceiling not Enclosed')

            elseif fail3 == 0 & skipcolumn == 0
                good=1;
              %  disp('Osteon Found')
                run local_sub04
            end
        else
        end
      end
```

```
   end


   save 'osteoncoord08A.txt' xy -ascii -tabs

% This algorithm checks the surrounding area for bone to
ensure that the area is an enclosed circle


    if bw(r-1,c-1) == 1
           ok1=0;
       else
            ok1=1;
  end

    if bw(r-1,c) == 1
            ok2=0;

    else
            ok2=1;
 end

    if bw(r-1,c+1) == 1
            ok3=0;
      else
            ok3=1;
end


        if (ok1 == 0 | ok2 == 0 | ok3 == 0)
            %disp('Area Not Enclosed')
            fail1=1;

        end







span=0;
y=c;

   while bw(r,y) == 1

        span=span+1;
```

```
    y=y+1;

    if span > limit
         fail2=1;
                break
end


    center=round(span/2);
    o=c+center-1;
    dc=o;
    xcenter=zeros(1,limit);
    xcenter(1)=dc;

end

 for s=1:(span+1)

     if bw(r-1,c+s) == 1
         fail3=1;
         break
     end

 end


for j=1:limit
     while good == 1

    left=0;
    right=0;


        for i=0:limit

            if bw(r+j,dc-i) == 1
                left=left+1;

            elseif bw(r+1,dc-i) == 0
                break
            end

            if bw(r+j,dc+i) == 1
                right=right+1;

            elseif bw(r+1,dc+i) == 0
                break
```

```
                end
             end

            xcenter(j+1)=(right-left) + dc;
               go=1;
               check=0;
                 dc=xcenter(j+1);
                 ocheck=0;
              run local_sub05

              if ocheck == 1
                     run local_sub06
                     break
              else
                    break

          end
       end
   end

while go == 1

    for t=(dc-(left)):(dc+(right))

        if bw(r+j+1,t) == 1
            go=1;
          check=1;
                break
          end
          end

         if check == 0
             go=0;
        %  disp('Bottom of Osteon')
          good=0;
          ocheck=1;
              break
          end

    if bw(r+j+1,dc) == 1
        dc=dc;
        go=0;
        break

    elseif bw(r+j+1,dc-1) == 1
        dc=dc-1;
        go=0;
```

```
        break

    elseif bw(r+j+1,dc+1) == 1
        dc=dc+1;
        go=0;
        break
    end

    for x=0:right

        if bw(r+j+1,dc+x) == 1
            dc=dc+x;
            go=0;
            break
        end
    end

    for w=0:left

        if bw(r+j+1,dc-w) == 1
            dc=dc-w;
            go=0;
            break
        end
    end
end
%disp('Determining Center Coordinates...')
xcenter;

rowsdown=0;

for v=1:length(xcenter)
    if xcenter(v) > 0
        xcoor=round(mean(xcenter(1:v)));
        rowsdown=rowsdown+1;
    end
end

ycoor=r+round(rowsdown/2)-1;

oc=oc+1

 xy(oc,:)=[ycoor,xcoor];
```

```
% This is a subroutine algorithm that defines the interior
and exterior regions of the rib
% specimen, and divedes the osteon coordinates as such

while done == 0;

xy1=load('rotatexy01.txt'); %save 'rotatexy01.txt' xy1   -
ascii -tabs
xy2=load('rotatexy02.txt'); %save 'rotatexy02.txt' xy2   -
ascii -tabs
xy3=load('rotatexy03.txt'); %save 'rotatexy03.txt' xy3   -
ascii -tabs
xy4=load('rotatexy04.txt'); %save 'rotatexy04.txt' xy4   -
ascii -tabs
xy5=load('rotatexy05.txt'); %save 'rotatexy05.txt' xy5   -
ascii -tabs
xy6=load('rotatexy06.txt'); %save 'rotatexy06.txt' xy6   -
ascii -tabs
xy7=load('rotatexy07.txt'); %save 'rotatexy07.txt' xy7   -
ascii -tabs
xy8=load('rotatexy08.txt'); %save 'rotatexy08.txt' xy8   -
ascii -tabs
xy9=load('rotatexy09.txt'); %save 'rotatexy09.txt' xy9   -
ascii -tabs

xy1=osteonc{1};
xy2=osteonc{2};
xy3=osteonc{3};
xy4=osteonc{4};
xy5=osteonc{5};
xy6=osteonc{6};
xy7=osteonc{7};
xy8=osteonc{8};
xy9=osteonc{9};



inmin=min(xy(:,1));
inmax=inmin+inth;
extmax=max(xy(:,1));
extmin=extmax-exth;


for w=1:9

    rc=osteonc{w};
   a=0;
```

```
   b=0;
for u=1:length(rc)
    if ((rc(u,1) >= inmin) & (rc(u,1) <= inmax))
        a=a+1;
        into(a,:)=rc(u,:);
    end

     if ((rc(u,1) >= extmin) & (rc(u,1) <= extmax))
         b=b+1;
        exto(b,:)=rc(u,:);
    end

end

intoxy{w}=into;
extoxy{w}=exto;
cintoxy(w)=mean(into(:,2));
cextoxy(w)=mean(exto(:,2));
into(:,:)=0;
exto(:,:)=0;

end
% Interior  surface osteon coordinates
for i=1:8

    ocorin01=intoxy{i};
    ocorin02=intoxy{i+1};
          c=0;
   for k=1:length(ocorin01)

    for j=1:length(ocorin02)

        if (abs(ocorin01(k,1)-ocorin02(j,1)) <= thresh &
abs(ocorin01(k,2)-ocorin02(j,2)) <= thresh)
            %(ocorin1(k,2) >= ((ocorin2(j,2)-thresh)) &
(ocorin1(k,2) <= (ocorin2(j,2)+thresh)) & (ocorin1(k,1) >=
(ocorin2(j,1)-thresh)) & (ocorin1(k,1) <=
(ocorin2(j,1)+thresh)))
           c=c+1;
                ocorin1n(c,:)=ocorin01(k,:);
                ocorin2n(c,:)=ocorin02(j,:);
           break
            end

        end
    end
```

```
        % extxy{i} and extxy01{i}  represent corresponding
osteons: these coordinates will be used to determine average
offset angle from bone axis
    intxy{i}=ocorin1n;
    intxy01{i}=ocorin2n;  %starts at slide two and ends at
eight
end
i=1;

% Exterior surface osteon coordinates
for i=1:8

    ocorex01=extoxy{i};
    ocorex02=extoxy{i+1};
          c=0;
   for k=1:length(ocorex01)

    for j=1:length(ocorex02)

        if (abs(ocorex01(k,1)-ocorex02(j,1)) <= thresh &
abs(ocorex01(k,2)-ocorex02(j,2)) <= thresh)
            %(ocorin1(k,2) >= ((ocorin2(j,2)-thresh)) &
(ocorin1(k,2) <= (ocorin2(j,2)+thresh)) & (ocorin1(k,1) >=
(ocorin2(j,1)-thresh)) & (ocorin1(k,1) <=
(ocorin2(j,1)+thresh)))
           c=c+1;
                ocorex1n(c,:)=ocorex01(k,:);
                ocorex2n(c,:)=ocorex02(j,:);
           break
            end

        end
    end
    % extxy{i} and extxy01{i}  represent corresponding
osteons: these coordinates will be used to determine average
offset angle from bone axis
    extxy{i}=ocorex1n;
    extxy01{i}=ocorex2n;  %starts at slide two and ends at
eight
end


%----------------------------------------- Interior
Coordinates ----------------------------------%
for i=1:8
    d=0;
    ocorin1=intxy{i};
```

```
    for j=1:length(ocorin1)

        if (ocorin1(j,1) ~= 0 & i == 1)
            d=d+1;
            ocorin11(d,:)=ocorin1(j,:);

         elseif (ocorin1(j,1) ~= 0 & i == 2)
        d=d+1;
        ocorin21(d,:)=ocorin1(j,:);

        elseif (ocorin1(j,1) ~= 0 & i == 3)
        d=d+1;
          ocorin3(d,:)=ocorin1(j,:);

         elseif (ocorin1(j,1) ~= 0 & i == 4)
        d=d+1;
        ocorin4(d,:)=ocorin1(j,:);

         elseif (ocorin1(j,1) ~= 0 & i == 5)
        d=d+1;
        ocorin5(d,:)=ocorin1(j,:);

         elseif (ocorin1(j,1) ~= 0 & i == 6)
        d=d+1;
        ocorin6(d,:)=ocorin1(j,:);

         elseif (ocorin1(j,1) ~= 0 & i == 7)
        d=d+1;
        ocorin7(d,:)=ocorin1(j,:);

        elseif (ocorin1(j,1) ~= 0 & i == 8)
        d=d+1;
        ocorin8(d,:)=ocorin1(j,:);

           end
    end

end
d2=length(ocorin21);
d3=length(ocorin3);
d4=length(ocorin4);
d5=length(ocorin5);
d6=length(ocorin6);
d7=length(ocorin7);
d8=length(ocorin8);
```

```
    d=0;
    i=1;
     for i=1:8

         ocorin2=intxy01{i};
             d=0;

     for j=1:length(ocorin2)

         if (ocorin2(j,1) ~= 0 & i == 1)
             d2=d2+1;
             ocorin21(d2,:)=ocorin2(j,:);

          elseif (ocorin2(j,1) ~= 0 & i == 2)
         d3=d3+1;
         ocorin3(d3,:)=ocorin2(j,:);

         elseif (ocorin2(j,1) ~= 0 & i == 3)
         d4=d4+1;
           ocorin4(d4,:)=ocorin2(j,:);

          elseif (ocorin2(j,1) ~= 0 & i == 4)
         d5=d5+1;
         ocorin5(d5,:)=ocorin2(j,:);

          elseif (ocorin2(j,2) ~= 0 & i == 5)
         d6=d6+1;
         ocorin6(d6,:)=ocorin2(j,:);

          elseif (ocorin2(j,1) ~= 0 & i == 6)
         d7=d7+1;
         ocorin7(d7,:)=ocorin2(j,:);

          elseif (ocorin2(j,1) ~= 0 & i == 7)
         d8=d8+1;
         ocorin8(d,:)=ocorin2(j,:);

         elseif (ocorin2(j,1) ~= 0 & i == 8)
         d=d+1;
         ocorin9(d,:)=ocorin2(j,:);

            end
     end

end
```

```
%--------------------------Exeterior Coordinates------------
------------------
d1=length(ocorin11);
d2=length(ocorin21);
d3=length(ocorin3);
d4=length(ocorin4);
d5=length(ocorin5);
d6=length(ocorin6);
d7=length(ocorin7);
d8=length(ocorin8);
d9=length(ocorin9);

   for i=1:8
    d=0;
    ocorex1=extxy{i};

    for j=1:length(ocorex1)

        if (ocorex1(j,1) ~= 0 & i == 1)
            d1=d1+1;
            ocorin11(d1,:)=ocorex1(j,:);

         elseif (ocorex1(j,1) ~= 0 & i == 2)
        d2=d2+1;
        ocorin21(d2,:)=ocorex1(j,:);

        elseif (ocorex1(j,1) ~= 0 & i == 3)
        d3=d3+1;
          ocorin3(d3,:)=ocorex1(j,:);

         elseif (ocorex1(j,1) ~= 0 & i == 4)
        d4=d4+1;
        ocorin4(d4,:)=ocorex1(j,:);

         elseif (ocorex1(j,1) ~= 0 & i == 5)
        d5=d5+1;
        ocorin5(d5,:)=ocorex1(j,:);

         elseif (ocorex1(j,1) ~= 0 & i == 6)
        d6=d6+1;
        ocorin6(d6,:)=ocorex1(j,:);

         elseif (ocorex1(j,1) ~= 0 & i == 7)
        d7=d7+1;
        ocorin7(d7,:)=ocorex1(j,:);

         elseif (ocorex1(j,1) ~= 0 & i == 8)
```

```
        d8=d8+1;
        ocorin7(d7,:)=ocorex1(j,:);

           end
    end

end
d1=length(ocorin11);
d2=length(ocorin21);
d3=length(ocorin3);
d4=length(ocorin4);
d5=length(ocorin5);
d6=length(ocorin6);
d7=length(ocorin7);
d8=length(ocorin8);

   d=0;
   i=1;
    for i=1:8

        ocorex2=extxy01{i};
            d=0;

    for j=1:length(ocorex2)

        if (ocorex2(j,1) ~= 0 & i == 1)
            d2=d2+1;
            ocorin21(d2,:)=ocorex2(j,:);

         elseif (ocorex2(j,1) ~= 0 & i == 2)
        d3=d3+1;
        ocorin3(d3,:)=ocorex2(j,:);

        elseif (ocorex2(j,1) ~= 0 & i == 3)
        d4=d4+1;
          ocorin4(d4,:)=ocorex2(j,:);

         elseif (ocorex2(j,1) ~= 0 & i == 4)
        d5=d5+1;
        ocorin5(d5,:)=ocorex2(j,:);

         elseif (ocorex2(j,2) ~= 0 & i == 5)
        d6=d6+1;
        ocorin6(d6,:)=ocorex2(j,:);

         elseif (ocorex2(j,1) ~= 0 & i == 6)
        d7=d7+1;
```

```
        ocorin7(d7,:)=ocorex2(j,:);

         elseif (ocorex2(j,1) ~= 0 & i == 7)
        d8=d8+1;
        ocorin8(d8,:)=ocorex2(j,:);


           end
    end

end


intxy2={ocorin11,ocorin21,ocorin3,ocorin4,ocorin5,ocorin6,oco
rin7,ocorin8};

    run local_image

break

end


int1=[intxy{1},intxy01{1}];
int2=[intxy{2},intxy01{2}];
int3=[intxy{3},intxy01{3}];
int4=[intxy{4},intxy01{4}];
int5=[intxy{5},intxy01{5}];
int6=[intxy{6},intxy01{6}];
int7=[intxy{7},intxy01{7}];
int8=[intxy{8},intxy01{8}];

ext1=[extxy{1},extxy01{1}];
ext2=[extxy{2},extxy01{2}];
ext3=[extxy{3},extxy01{3}];
ext4=[extxy{4},extxy01{4}];
ext5=[extxy{5},extxy01{5}];
ext6=[extxy{6},extxy01{6}];
ext7=[extxy{7},extxy01{7}];
ext8=[extxy{8},extxy01{8}];

save 'int1.txt' int1   -ascii -tabs
save 'int2.txt' int2   -ascii -tabs
save 'int3.txt' int3   -ascii -tabs
save 'int4.txt' int4   -ascii -tabs
save 'int5.txt' int5   -ascii -tabs
save 'int6.txt' int6   -ascii -tabs
```

```
save 'int7.txt' int7   -ascii -tabs
save 'int8.txt' int8   -ascii -tabs

save 'ext1.txt' ext1   -ascii -tabs
save 'ext2.txt' ext2   -ascii -tabs
save 'ext3.txt' int3   -ascii -tabs
save 'ext4.txt' ext4   -ascii -tabs
save 'ext5.txt' ext5   -ascii -tabs
save 'ext6.txt' ext6   -ascii -tabs
save 'ext7.txt' ext7   -ascii -tabs
save 'ext8.txt' ext8   -ascii -tabs
```

```
%The algorithm below searches through osteon coordinates and
determines which
%series of coordinates correspond to a single haversian canal.

clear
clc

int1=load('int1.txt');
int2=load('int2.txt');
int3=load('int3.txt');
int4=load('int4.txt');
int5=load('int5.txt');
int6=load('int6.txt');
int7=load('int7.txt');

ext1=load('ext1.txt');
ext2=load('ext2.txt');
ext3=load('ext3.txt');
ext4=load('ext4.txt');
ext5=load('ext5.txt');
ext6=load('ext6.txt');
ext7=load('ext7.txt');


int11=[int1(:,1),int1(:,2)];    int12=[int1(:,3),int1(:,4)];
int21=[int2(:,1),int2(:,2)];    int22=[int2(:,3),int2(:,4)];
int31=[int3(:,1),int3(:,2)];    int32=[int3(:,3),int3(:,4)];
int41=[int4(:,1),int4(:,2)];    int42=[int4(:,3),int4(:,4)];
int51=[int5(:,1),int5(:,2)];    int52=[int5(:,3),int5(:,4)];
int61=[int6(:,1),int6(:,2)];    int62=[int6(:,3),int6(:,4)];
int71=[int7(:,1),int7(:,2)];    int72=[int7(:,3),int7(:,4)];

internal01={int11,int21,int31,int41,int51,int61,int71};
internal02={int12,int22,int32,int42,int52,int62,int72};
a=0; b=0; c=0; d=0; e=0; f=0;

for i=1:6

    for j=1:length(internal02{i})

        int011=internal01{i};
        int01=internal01{i+1};
        int02=internal02{i};
        int022=internal02{i+1};

            for k=1:length(int01)
```

```
                                    if int02(j,1) == 0
                                        break

                                    elseif int02(j,1) ==
int01(k,1) & i == 1
                                    a=a+1;

coor01{a}=[int011(j,:);int02(j,:);int022(k,:)];
                                    elseif int02(j,1) ==
int01(k,1) & i == 2
                                    b=b+1;

coor02{b}=[int011(j,:);int02(j,:);int022(k,:)];
                                    elseif int02(j,1) ==
int01(k,1) & i == 3
                                    c=c+1;

coor03{c}=[int011(j,:);int02(j,:);int022(k,:)];
                                    elseif int02(j,1) ==
int01(k,1) & i == 4
                                    d=d+1;

coor04{d}=[int011(j,:);int02(j,:);int022(k,:)];
                                    elseif int02(j,1) ==
int01(k,1) & i == 5
                                    e=e+1;

coor05{e}=[int011(j,:);int02(j,:);int022(k,:)];
                                    elseif int02(j,1) ==
int01(k,1) & i == 6
                                    f=f+1;

coor06{f}=[int011(j,:);int02(j,:);int022(k,:)];
                                        %elseif int02(j,1) ==
int01(k,1) & i == 7
                                     %
coor07{k}=[int011(j,:);int02(j,:);int022(k,:)];
                        end
                    end
                end
            end

                i=1;

                     for  i=1:2:length(coor01)
                     coor01n(1:3,i:i+1)=coor01{i};      save
'intcon1.txt' coor01n    -ascii -tabs
```

```
                end
                for i=1:2:length(coor02)
                    coor02n(1:3,i:i+1)=coor02{i};      save
'intcon2.txt' coor02n    -ascii -tabs
                end
                for i=1:2:length(coor03)
                    coor03n(1:3,i:i+1)=coor03{i};      save
'intcon3.txt' coor03n    -ascii -tabs
                end
                for i=1:2:length(coor04)
                    coor04n(1:3,i:i+1)=coor04{i};      save
'intcon4.txt' coor04n    -ascii -tabs
                end
                %for i=1:2:length(coor05)
                %    coor05n(1:3,i:i+1)=coor05{i};      save
'intcon5.txt' coor05n    -ascii -tabs
                %end
                %for i=1:2:length(coor06)
                %    coor06n(1:3,i:i+1)=coor06{i};      save
'intcon6.txt' coor06n    -ascii -tabs
                %end

                    %coor07n(1:3,i:i+1)=coor07{i};

ext11=[ext1(:,1),ext1(:,2)];    ext12=[ext1(:,3),ext1(:,4)];
ext21=[ext2(:,1),ext2(:,2)];    ext22=[ext2(:,3),ext2(:,4)];
ext31=[ext3(:,1),ext3(:,2)];    ext32=[ext3(:,3),ext3(:,4)];
ext41=[ext4(:,1),ext4(:,2)];    ext42=[ext4(:,3),ext4(:,4)];
ext51=[ext5(:,1),ext5(:,2)];    ext52=[ext5(:,3),ext5(:,4)];
ext61=[ext6(:,1),ext6(:,2)];    ext62=[ext6(:,3),ext6(:,4)];
ext71=[ext7(:,1),ext7(:,2)];    ext72=[ext7(:,3),ext7(:,4)];

external01={ext11,ext21,ext31,ext41,ext51,ext61,ext71};
external02={ext12,ext22,ext32,ext42,ext52,ext62,ext72};

a=0; b=0; c=0; d=0; e=0; f=0;

for i=1:6

    for j=1:length(external02{i})

        ext011=external01{i};
        ext01=external01{i+1};
        ext02=external02{i};
        ext022=external02{i+1};

            for k=1:length(ext01)
```

```
                                    if ext02(j,1) == 0
                                       break
                                    elseif ext02(j,1) ==
ext01(k,1) & i == 1
                                    a=a+1;

coorex01{a}=[ext011(j,:);ext02(j,:);ext022(k,:)];
                                    break
                                    elseif ext02(j,1) ==
ext01(k,1) & i == 2
                                    b=b+1;

coorex02{b}=[ext011(j,:);ext02(j,:);ext022(k,:)];
                                       break
                                    elseif ext02(j,1) ==
ext01(k,1) & i == 3
                                    c=c+1;

coorex03{c}=[ext011(j,:);ext02(j,:);ext022(k,:)];
                                       break
                                    elseif ext02(j,1) ==
ext01(k,1) & i == 4
                                    d=d+1;

coorex04{d}=[ext011(j,:);ext02(j,:);ext022(k,:)];
                                       break
                                    elseif ext02(j,1) ==
ext01(k,1) & i == 5
                                    e=e+1;

coorex05{e}=[ext011(j,:);ext02(j,:);ext022(k,:)];
                                       break
                                    elseif ext02(j,1) ==
ext01(k,1) & i == 6
                                    f=f+1;

coorex06{f}=[ext011(j,:);ext02(j,:);ext022(k,:)];
                                       break
                                       %elseif int02(j,1) ==
int01(k,1) & i == 7
                                     %
coor07{k}=[int011(j,:);int02(j,:);int022(k,:)];
                           end
                       end
                   end
               end
```

```
                i=1;

                   for  i=1:2:length(coorex01)
                   coorex01n(1:3,i:i+1)=coorex01{i};
save 'extcon1.txt' coorex01n    -ascii -tabs
                  end

                   for i=1:2:length(coorex02)
                      coorex02n(1:3,i:i+1)=coorex02{i};
save 'extcon2.txt' coorex02n    -ascii -tabs
                  end

                 for i=1:2:length(coorex03)
                     coorex03n(1:3,i:i+1)=coorex03{i};
save 'extcon3.txt' coorex03n    -ascii -tabs
                 end
                  for i=1:2:length(coorex04)
                      coorex04n(1:3,i:i+1)=coorex04{i};
save 'extcon4.txt' coorex04n    -ascii -tabs
                  end
                  for i=1:2:length(coorex05)
                      coorex05n(1:3,i:i+1)=coorex05{i};
save 'extcon5.txt' coorex05n    -ascii -tabs
                  end
                  for i=1:2:length(coorex06)
                      coorex06n(1:3,i:i+1)=coorex06{i};
save 'extcon6.txt' coorex06n    -ascii -tabs
                  end

                      %coor07n(1:3,i:i+1)=coor07{i};
```

```
% The algorithm below creates images of the osteon
coordinates, represented by white dots
% This is performed for each histological image

bwo=imread('01A','tif');

j=1;
i=1;
for j=1:9

xy=intxy2{j};
bwo(:,:)=0;
disp('Here we go')
for i=1:length(xy)

       bwo(xy(i,1),xy(i,2))=1;
       bwo(xy(i,1)+1,xy(i,2))=1;
       bwo(xy(i,1)-1,xy(i,2))=1;
       bwo(xy(i,1),xy(i,2)+1)=1;
       bwo(xy(i,1),xy(i,2)-1)=1;
       bwo(xy(i,1)+2,xy(i,2))=1;
       bwo(xy(i,1)-2,xy(i,2))=1;
       bwo(xy(i,1),xy(i,2)+2)=1;
       bwo(xy(i,1),xy(i,2)-2)=1;

       bwo(xy(i,1)+1,xy(i,2)+1)=1;
       bwo(xy(i,1)-1,xy(i,2)+1)=1;
       bwo(xy(i,1)+1,xy(i,2)-1)=1;
       bwo(xy(i,1)-1,xy(i,2)-1)=1;
       bwo(xy(i,1)+2,xy(i,2)+2)=1;
       bwo(xy(i,1)-2,xy(i,2)+2)=1;
       bwo(xy(i,1)+2,xy(i,2)-2)=1;
       bwo(xy(i,1)-2,xy(i,2)-2)=1;

   end

       if j == 1
       imwrite(bwo,'Osteonmap01.tif','tif');
       elseif j == 2
       imwrite(bwo,'Osteonmap02.tif','tif');
       elseif j == 3
       imwrite(bwo,'Osteonmap03.tif','tif');
       elseif j == 4
       imwrite(bwo,'Osteonmap04.tif','tif');
       elseif j == 5
       imwrite(bwo,'Osteonmap05.tif','tif');
       elseif j == 6
```

```
       imwrite(bwo,'Osteonmap06.tif','tif');
       elseif j == 7
       imwrite(bwo,'Osteonmap07.tif','tif');
       elseif j == 8
      imwrite(bwo,'Osteonmap08.tif','tif');
      elseif j == 9
      imwrite(bwo,'Osteonmap09.tif','tif');
   end
end


done=1;
%The algorithm below creates images of the osteon coordinates
represented as dots,
%This is also a subroutine for a master algorithm.

for j=1:9

       xy=osteoncoor{j}';
       xy=[xy(:,1),xy(:,2)];
           m=ones(length(xy),1);
           fc=m.*fcol;
           fr=m.*frow;
           fr=fr;%.*.75;
           fc=fc;%.*.75;
           move=[fr,fc];
           xy=xy-move;
           osteonc{j}=xy;


bwo=imread('template','tif');
bwo(:,:)=0;
disp('Here we go')
for i=1:length(xy)

       bwo(xy(i,1),xy(i,2))=1;
       bwo(xy(i,1)+1,xy(i,2))=1;
       bwo(xy(i,1)-1,xy(i,2))=1;
       bwo(xy(i,1),xy(i,2)+1)=1;
       bwo(xy(i,1),xy(i,2)-1)=1;
       bwo(xy(i,1)+2,xy(i,2))=1;
       bwo(xy(i,1)-2,xy(i,2))=1;
       bwo(xy(i,1),xy(i,2)+2)=1;
       bwo(xy(i,1),xy(i,2)-2)=1;

       bwo(xy(i,1)+1,xy(i,2)+1)=1;
       bwo(xy(i,1)-1,xy(i,2)+1)=1;
```

```
        bwo(xy(i,1)+1,xy(i,2)-1)=1;
        bwo(xy(i,1)-1,xy(i,2)-1)=1;
        bwo(xy(i,1)+2,xy(i,2)+2)=1;
        bwo(xy(i,1)-2,xy(i,2)+2)=1;
        bwo(xy(i,1)+2,xy(i,2)-2)=1;
        bwo(xy(i,1)-2,xy(i,2)-2)=1;

    end


    if j == 1
        imwrite(bwo,'allcoordinates1.tif','tif');
        elseif j == 2
 imwrite(bwo,'allcoordinates2.tif','tif');
  elseif j == 3
 imwrite(bwo,'allcoordinates3.tif','tif');
end
  end
```

```
%The algorithm below rotates the osteons coordinates from all
images of a
%single rib specimen into a single reference frame.
clear
clc


dataset=load('datum.txt');
coor1=load('osteoncoord01a.txt');
coor2=load('osteoncoord02a.txt');
coor3=load('osteoncoord03a.txt');
coor4=load('osteoncoord04a.txt');
coor5=load('osteoncoord05a.txt');
coor6=load('osteoncoord06a.txt');
coor7=load('osteoncoord07a.txt');
coor8=load('osteoncoord08a.txt');
offsetdeg=dataset(1,5);
inth=dataset(2,5);  % interior surface thickness
space=dataset(3,5);
exth=dataset(4,5); % exterioro surface thickness
thresh=20;
coorall={coor1,coor2,coor3,coor4,coor5,coor6,coor7,coor8};
done=0;

datum1=dataset(:,1:2);
datum2=dataset(:,3:4);

%ozeros=zeros(length(coor),1);
%oones=ones(length(coor),1);

line12=datum2-datum1;
%lineo=osteon-datum1;

%Determine magnitudes:
    for i=1:8

        magdatum1(i)=sqrt(datum1(i)^2+datum1(i,2)^2);
        magdatum2(i)=sqrt(datum2(i)^2+datum2(i,2)^2);
        magline12(i)=sqrt(line12(i)^2+line12(i,2)^2);
        %magline1o(i)=sqrt(lineo(i)^2+lineo(i,2)^2);

end
i=0;

hor=[1 0];
```

```
%angle offset with horizontal axis for x axis created by the
two datum points
offset=zeros(1,8);
for i=1:8

offset(i)=(atan(line12(i,2)/line12(i,1))+(offsetdeg*pi/180));
    end
i=0;

%rot1 through rot 8 are the rotation matrices for each image

for i=1:8
rot{i}=[cos(offset(i)),-
sin(offset(i)),0;sin(offset(i)),cos(offset(i)),0;0,0,1;0,0,0]
;
end
i=0;

%Homogeneous Transform: rotates and moves individual image
axis to the reference plane (0,0)

transdatum1=zeros(8,4);
transdatum1(:,1)=datum1(:,1);
transdatum1(:,2)=datum1(:,2);
transdatum1(:,4)=1;

for i=1:8
trans{i}=[rot{i},transdatum1(i,:)'];
end

for j=1:8
    ozeros{j}=zeros(length(coorall{j}),1);
    oones{j}=ones(length(coorall{j}),1);
   coorall{j}=[coorall{j},ozeros{j},oones{j}];
      end

% New osteon coordinates with repect to 0,0 axis


for i=1:8
    osteoncoor{i}=(trans{i}*coorall{i}');
end

oscoor1=osteoncoor{1}';
oscoor1=[oscoor1(:,1),oscoor1(:,2)];

frow=min(oscoor1(:,1))-100;
```

```
fcol=min(oscoor1(:,2))-205;

 j=1;

   for j=1:8

       xy=osteoncoor{j}';
       xy=[xy(:,1),xy(:,2)];
           m=ones(length(xy),1);
           fc=m.*fcol;
           fr=m.*frow;
           fr=fr;
           fc=fc;
           move=[fr,fc];
           xy=xy-move;
           osteonc{j}=xy;
       end

inmin=min(xy(:,1));
inmax=inmin+inth;
extmax=max(xy(:,1));
extmin=extmax-exth;


for w=1:8

    rc=osteonc{w};
   a=0;
   b=0;
for u=1:length(rc)
    if ((rc(u,1) >= inmin) & (rc(u,1) <= inmax))
        a=a+1;
        into(a,:)=rc(u,:);
    end

     if ((rc(u,1) >= extmin) & (rc(u,1) <= extmax))
         b=b+1;
        exto(b,:)=rc(u,:);
    end

end
intoxy{w}=into;
extoxy{w}=exto;
cintoxy(w)=mean(into(:,2));
cextoxy(w)=mean(exto(:,2));
into(:,:)=0;
exto(:,:)=0;
```

```
end
% Interior  surface osteon coordinates
for i=1:7

    ocorin01=intoxy{i};
    ocorin02=intoxy{i+1};
          c=0;
   for k=1:length(ocorin01)

    for j=1:length(ocorin02)

        if (abs(ocorin01(k,1)-ocorin02(j,1)) <= thresh &
abs(ocorin01(k,2)-ocorin02(j,2)) <= thresh)
            %(ocorin1(k,2) >= ((ocorin2(j,2)-thresh)) &
(ocorin1(k,2) <= (ocorin2(j,2)+thresh)) & (ocorin1(k,1) >=
(ocorin2(j,1)-thresh)) & (ocorin1(k,1) <=
(ocorin2(j,1)+thresh)))
           c=c+1;
                ocorin1n(c,:)=ocorin01(k,:);
                ocorin2n(c,:)=ocorin02(j,:);
           break
            end

        end
    end
        % extxy{i} and extxy01{i}  represent corresponding
osteons: these coordinates will be used to determine average
offset angle from bone axis
    intxy{i}=ocorin1n;
    intxy01{i}=ocorin2n;  %starts at slide two and ends at
eight
end
i=1;

% Exterior surface osteon coordinates
for i=1:7

    ocorex01=extoxy{i};
    ocorex02=extoxy{i+1};
          c=0;
   for k=1:length(ocorex01)

    for j=1:length(ocorex02)

        if (abs(ocorex01(k,1)-ocorex02(j,1)) <= thresh &
abs(ocorex01(k,2)-ocorex02(j,2)) <= thresh)
```

```
            %(ocorin1(k,2) >= ((ocorin2(j,2)-thresh)) &
(ocorin1(k,2) <= (ocorin2(j,2)+thresh)) & (ocorin1(k,1) >=
(ocorin2(j,1)-thresh)) & (ocorin1(k,1) <=
(ocorin2(j,1)+thresh)))
           c=c+1;
                ocorex1n(c,:)=ocorex01(k,:);
                ocorex2n(c,:)=ocorex02(j,:);
           break
            end

        end
    end
    % extxy{i} and extxy01{i}  represent corresponding
osteons: these coordinates will be used to determine average
offset angle from bone axis
    extxy{i}=ocorex1n;
    extxy01{i}=ocorex2n;  %starts at slide two and ends at
eight
end

int1=[intxy{1},intxy01{1}];
int2=[intxy{2},intxy01{2}];
int3=[intxy{3},intxy01{3}];
int4=[intxy{4},intxy01{4}];
int5=[intxy{5},intxy01{5}];
int6=[intxy{6},intxy01{6}];
int7=[intxy{7},intxy01{7}];

ext1=[extxy{1},extxy01{1}];
ext2=[extxy{2},extxy01{2}];
ext3=[extxy{3},extxy01{3}];
ext4=[extxy{4},extxy01{4}];
ext5=[extxy{5},extxy01{5}];
ext6=[extxy{6},extxy01{6}];
ext7=[extxy{7},extxy01{7}];

save 'int1.txt' int1   -ascii -tabs
save 'int2.txt' int2   -ascii -tabs
save 'int3.txt' int3   -ascii -tabs
save 'int4.txt' int4   -ascii -tabs
save 'int5.txt' int5   -ascii -tabs
save 'int6.txt' int6   -ascii -tabs
save 'int7.txt' int7   -ascii -tabs

save 'ext1.txt' ext1   -ascii -tabs
save 'ext2.txt' ext2   -ascii -tabs
save 'ext3.txt' ext3   -ascii -tabs
```

```
save 'ext4.txt' ext4   -ascii -tabs
save 'ext5.txt' ext5   -ascii -tabs
save 'ext6.txt' ext6   -ascii -tabs
save 'ext7.txt' ext7  -ascii -tabs
```

Vita

Joseph Michael Cormier

Joseph Cormier was born in Ruidoso, New Mexico on July 15, 1978. He attended Gadsden High School in Anthony NM. He graduated from the New Mexico Institute of Mining and Technology with a Bachelor's in Mechanical Engineering. Then moved to Virginia where he obtained his Master's in Mechanical Engineering with a Biomedical Engineering option at Virginia Polytechnic and State University. There he received an Outstanding Researcher award for the MS category at the 1st Annual Center for Biomedical Engineering Symposium at Virginia Tech. He also received the Impact Biomechanics Award for outstanding researcher in 2002. In 2003 he won first place in the Torgersen competition for outstanding researcher in the MS category for the School of Engineering at Virginia Tech. His research work conducted at the Impact Biomechanics Lab was published in automotive safety and biomechanical journals and conferences. The focus of his research was human tolerances to dynamic loading particularly related to automotive, sports and military applications. In July of 2003 he will begin his career in injury biomechanics working with an expert witness and research corporation. He has plans to pursue a PhD in Mechanical Engineering through a distance learning program at Virginia Tech. Eventually, he would like to be a teaching professor. During his free time, Joseph likes to play acoustic guitar, soccer, read and enjoy the outdoors.

Joseph Cormier can be contacted at the permanent address:

623 Sagewood
Chaparral NM 88081

_____
Joseph Cormier